This document was prepared in conjunction with work accomplished under Contract No. DE-AC09-96SR18500 with the U. S. Department of Energy.

DISCLAIMER

Keywords: Adsorption
High Level Waste
Kinetics
Thermodynamics

Prediction Models for Plutonium, Strontium, Uranium and Neptunium Loading onto Monosodium Titanate (MST)

F. F. Fondeur
D. T. Hobbs
M. J. Barnes
T. B. Peters
S. D. Fink

Publication date: July 11, 2005

Westinghouse Savannah River Company
Savannah River Site
Aiken, SC 29808

Prepared for the U.S. Department of Energy Under Contract Number DE-AC09-96SR18500

APPROVALS

Authors

Fernando Fondeur — 7.13.05
F. F. Fondeur, Waste Processing Technology — Date

D. T. Hobbs — 7/19/05
D. T. Hobbs, Waste Processing Technology — Date

M. J. Barnes — 7/14/05
M. J. Barnes, Waste Processing Technology — Date

Thomas B. Peters — 7/13/2005
T. B. Peters, Waste Processing Technology — Date

Samuel D. Fink — 7/13/2005
S. D. Fink, Manager, SRNL, Liquid Waste Processing Group — Date

Technical Evaluator

Michael R Poirier — 7/19/05
M. R. Poirier, Waste Processing Technology — Date

Management

J. C. Griffin — 7/21/05
J. C. Griffin, Manager, SRNL, Waste Processing Technology Section — Date

Customer Concurrence

Harry D. Harmon — 7/25/05
H. D. Harmon, SPP Technology Development Manager — Date

7/27/05
A. J. ~~Tizler~~, Actinide Removal Project — Date

Tisler
7/28/05
W. L. Isom, Jr., Manager, Salt Disposition Engineering — Date

Patricia C. Suggs — 7-28-05
P. C. Suggs, DOE-AMWD Technology Development Lead — Date

CONTENTS

LIST OF FIGURES

LIST OF TABLES

ACRONYM LIST

$q(t)$	Amount of radionuclide on MST at time t (μmoles/grams of MST)
q_{eq}	Equilibrium amount of radionuclide on MST (μmoles/grams of MST)
q_{eq}^{mx}	Maximum equilibrium amount of radionuclide on MST (μmoles/grams of MST)
R	Gas constant (=8.3145 Joules/mole •K)
T	Temperature (•K)
E	Absorption Activation energy (Joules/mole)
$\bullet\ E$	Activation energy (Joules/mole)
n	Exponent value (integer value)
S	The maximum radionuclide concentration studied or solubility
k	Rate constant (hour $^{-n}$)
k_o	Rate constant at a very high temperature (usually boiling temperature)
[MST]	Monosodium Titanate concentration (grams/liter)
$DF(t)$	Decontamination Factor at time t
DF_{eq}	Equilibrium Decontamination Factor
$ArcTan$	Inverse of the tangent function (degrees)
a, b	Constants (real values)
Ln	Natural Logarithm
C_{bulk}	Radionuclide concentration in solution away from the MST particles
D	Diffusion constant (cm^2/sec)
$\bullet/\bullet X$	Partial derivative with respect to X
d/dt	Ordinary derivative with respect to time
t	Time variable
T	Temperature variable

SUMMARY

The DA isotherm parameters for U, Pu, Sr and Np have been updated to include additional data obtained since the original derivation. The DA isotherms were modified to include a kinetic function derived by Rahn to describe sorbate loading from the beginning of sorption up to equilibrium. The final functions describe both kinetic and thermodynamic sorption. We selected the Rahn function to describe radionuclide sorption because it originates from diffusion and absorption controlled sorption. An investigation of the thermal behavior of radionuclide sorption on MST as shown by this data revealed the sorption process is diffusion (or transport) controlled (in solution). Transport in solution can in theory be accelerated by vigorous mixing but the range of available mixing speed in the facility design will probably not be sufficient to markedly increase radionuclide sorption rate on MST from diffusion-controlled sorption.[1] The laboratory studies included mixing energies hydraulically-scaled to match those of the Actinide Removal Process and these likely approximate the range of energies available in the Salt Waste Processing Facility.

1.0 Introduction

The Salt Waste Processing Facility (SWPF) and the Actinide Removal Process (ARP) will treat salt solution from the Savannah River Site (SRS) waste tanks that contain actinide levels in excess of the Saltstone Waste Acceptance Criteria (WAC). The treatment includes removal of ^{90}Sr and alpha-emitting ($^{238,239,240}Pu$, ^{237}Np) radionuclides from salt solution. The baseline technology features contacting the liquid waste with a sorbent (monosodium titanate (MST)) in a tank (batch mode). The rate and extent of Pu removal by MST sets the SWPF footprint and establishes cycle time and throughput for the ARP. To increase throughput and optimize the process, a predictive tool for actinide removal with MST is required. To this end, a previous study fit several isotherm functions to existing data for sorption of actinides on MST sorption data.[2] That study demonstrated that the Dubinin-Astashov (DA) function fit the sorption data best.

Since the completion of that work, new actinide adsorption data has been collected.[3,4] This paper incorporates the new data with the previous databank and recalculated the DA parameters. In addition, this paper develops a predictive tool for estimating actinide removal from liquid waste as a function of time. The final equation predicts both actinide concentration as a function of time and equilibrium (steady state) concentrations.

2.0 Analysis

The recently conducted MST tests generated 44 additional data points. This data was integrated into the databank[2] and re-checked for mass balance consistency. The data was further checked for sorption competition (for example if the presence of one radionuclide affects the sorption of others). We performed correlation tests between the equilibrium sorption of a radionuclide on MST and the concentration of the remaining radionuclides.

A negative correlation result is evidence of sorption competition. This finding allows fitting sorption data with functions that only include the radionuclide being studied.

The equilibrium sorption data was re-fitted with a DA function. The fitting procedure included a non-linear square fitting (minimizing the Sum of Square Errors) that used the Newton-Raphson searching criteria. Convergence was reached when either the objective (i.e., the sum of the square difference between the prediction from the DA function and the sorption data), parameter change or gradient of change was less than 10^{-6}. A similar criterion was used for fitting the kinetic sorption data to different kinetic functions.

To predict the MST concentration needed for a given decontamination factor (DF) value, we combined the Dubinin-Astashov equation with the mass balance equation. The Dubinin-Astashov equation follows.[5]

$$q_{eq} = q_{eq}^{\mathrm{mx}} \times e^{-\left(\frac{RT}{E} Ln\left(\frac{S}{[actinide]_{eq}}\right)\right)^n} \qquad 1$$

In this expression, q_{eq}^{mx} is the maximum strontium or actinide loaded on MST (given in μmole/g), *E* is the adsorption energy (J/mole), *R* is the gas constant (J/mole•K) and *S* is the maximum radionuclide concentration in solution tested.

One can express the mass balance equation between actinide in solution, on MST and the starting original concentration as shown in equation 2.

$$q_{eq} = \frac{[sorbate]_{initial}}{[MST]} \times \left(1 - \frac{1}{DF_{\mathrm{eq}}}\right) \qquad 2$$

In this expression, $[sorbate]_{initial}$ stands for the initial actinide concentration with μmolar units (before MST addition), [MST] is MST concentration in grams/L and *DF* stands for decontamination factor. Combining equations (1) and (2) leads to the following expression.

$$[MST] = \frac{[sorbate]_{initial}}{q_{eq}^{\mathrm{mx}}} \times \left[1 - \frac{1}{DF_{eq}}\right] \times e^{\left(\frac{RT}{E}\right)^n \times \left[Ln\left(\frac{S \times DF_{eq}}{[sorbate]_{initial}}\right)\right]^n} \qquad 3$$

From equation (3) given an initial sorbate concentration and desired decontamination factor, the MST concentration is easily obtained. The values for the other variables (such as maximum equilibrium loading, "*E*", "*S*", and "*n*" depend on the radionuclide as are given in Appendix B. Conversely, given an initial sorbate and MST concentration, the equation also provides the resulting decontamination factor.

To predict the "DF" value as a function of time, we rearranged the mass balance (equation 2) in terms of the equilibrium DF and sorbate loadings at equilibrium and time "t" as shown in equation 4.

$$DF(t) = \frac{1}{1 - \left(1 - \frac{1}{DF_{eq}}\right) \times \frac{q(t)}{q_{eq}}} \qquad 4$$

In this expression "$q(t)/q_{eq}$" (the extent of loading to equilibrium) is the kinetic function describing how much sorbate loads on MST as a function time. One of the purposes of this work is to find a kinetic adsorption function for actinide sorption on MST that can be inserted in equation (4). A literature search identified several kinetic functions for adsorption processes. Table 1 provides a list of the functions evaluated in this report. Table 2 provides the kinetic expressions for each of the functions listed in Table 1. For example, inserting the Rahn function to equation 4 yields a temporal DF equation as shown in equation 5.

$$DF(t) = \frac{1}{1 - \left(1 - \frac{1}{DF_{eq}}\right) \times \left[1 - e^{-kt^n}\right]} \qquad 5$$

Table 1. The kinetic functions considered for fitting actinide loading.

Model	Parameters	Number of Mathematical Operations	Formula	Reference
First order	2	5	$q = q_{eq}(1-e^{-kt})$	4
Second order	2	5	$q = q_{eq}(1-1/(1+kt))$	5
Ritchie	3	6	$q = q_{eq}(1-(1/(1+kt))^{n})$	6
Elovich	2	4	$q = q_{eq}Ln(at+1)$	7
Diffusion Limited	1	2	$q = bt^{1/2}$	10, 11
Power**	2	2	$q = bt^{n}$	6
Rahn	3	6	$q = q_{eq}(1-\exp(-kt^{n}))$	8, 9
Rudzinski	4	11	$q = q_{eq}(a \times Arctan(bt))^{n}/(1+ (a \times Arctan(bt))^{n})$	4

*In this table "k" stands for the rate constant, "t" stands for time, and "a and b" are constants.
** Power model is an empirical function for fitting sorption data that did not originated from a kinetic expression

Table 2. Rate of loading equations for the kinetic expressions.

Model	Kinetic Expression for rate of loading dq/dt
First Order[7]	$k(q_{eq}-q)$
Second Order[8]	$k(q_{eq}-q)^{2}$
Ritchie[9]	$k(q_{eq}-q)^{n}$
Elovich[10]	$\exp(-bq)$
Rahn[11,12]	$k(q_{eq}-q)/t^{n}$
Rudzinski[7]	$K(q_{eq}-q)^{n}/q^{n}$
Diffusion[13,14]	$D(\bullet C/\bullet X)_{0}$

The current strategy is to compute the equilibrium DF using equation 3 given an initial sorbate concentration and MST concentration or the MST concentrations given an initial sorbate concentration. Then the temporal changes of DF are computed using equation 4 (or 5 for example). A diagram of the calculation steps required for predicting DF as a function time is shown in Figure 1.

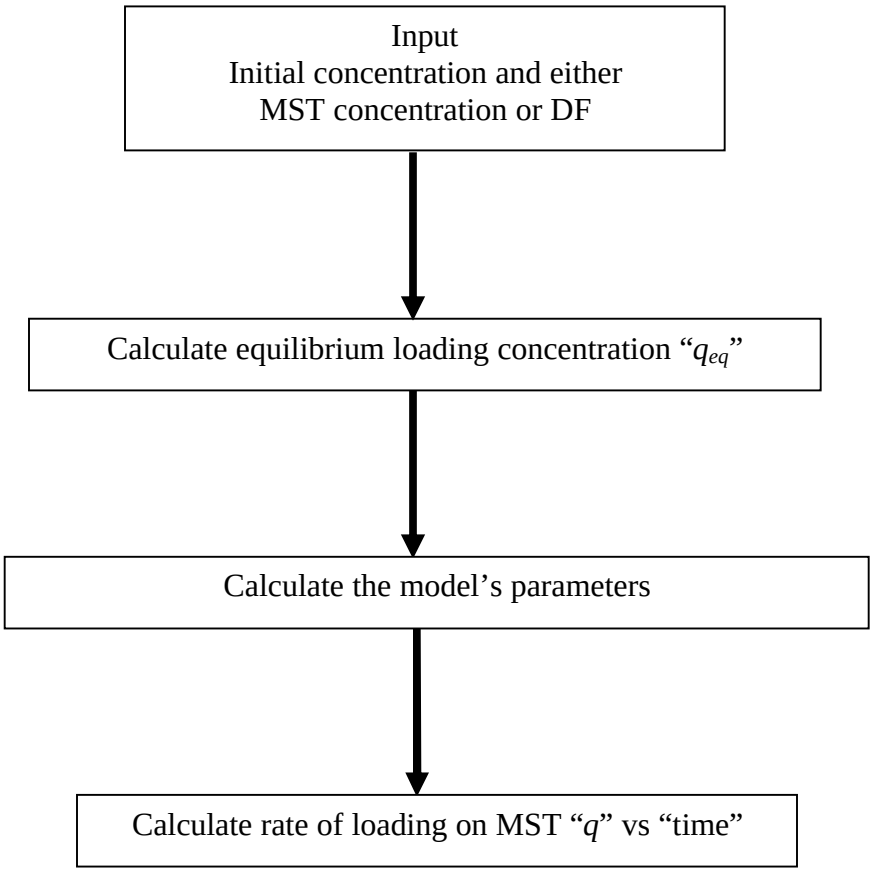

Figure 1. Schematic of the calculation step needed to predict DF as a function of time

When loading is controlled by both diffusion and adsorption, a non-analytical solution (by numerical integration) can be obtained. Only in the case of flux-controlled loading at the surface of MST, can an analytical solution can be obtained as shown below.

$$\frac{dq}{dt} = D\frac{\partial C}{\partial X} \text{ at the surface.} \qquad \frac{\partial C}{\partial X} = \frac{C_{bulk}}{\sqrt{\pi Dt}} \text{ for semi-infinite plane diffusion}$$

$$q = \frac{2D^{1/2}C_{bulk}}{\pi^{1/2}}t^{1/2}$$

In this expression, D stands for diffusion, C_{bulk} stands for bulk concentration and t stands for time.

Researchers felt the functions listed in Table 1 were sufficient to fit the data without the need for using rigorous numerical solutions to the coupled diffusion-adsorption kinetic equation. Please note that successfully fitting sorption data with an exponential function does not necessarily imply first order rate sorption. For example, mathematical analysis of a sorption test carried out under the conditions of a boundary layer (i.e., diffusion

controlled) around the sorbent also predicts an exponential function dependence on sorbate sorption.

The correlation coefficient (R^2) and standard error (SE) were computed to show the goodness of the fit. The R^2 and SE definitions follow.

$$R^2 = 1 - \frac{\sum (Experiment\ value - Model\ \ prediction)^2}{\sum (Experiment\ value - Mean\ of\ experiment\ values)^2} \qquad 7$$

$$SE = \sqrt{\frac{\sum (Experiment\ value - Model\ \ prediction)^2}{\#\ of\ \ data\ points - \#\ of\ \ parameters\ in\ the\ model}} \qquad 8$$

3.0 Results

3.1 Recalculation of the Equilibrium Dubinin-Astashov Parameters and Adsorption Enthalpy

Researchers added the more recent data on strontium and actinide sorption with the previous dataset and calculated new DA parameters as described in the Analysis section. Details of the DA refitting results for strontium and the actinides are shown in Appendix A. The DA expressions for Sr, Pu, U and Np are shown in equations 9 – 12, respectively. All sorbate concentrations are shown in units of micromoles per liter (μM) and loadings of sorbates onto MST in units of micromoles per gram of MST (μmole/g). Equations 9-12 represent the best DA function fit to a database that contains 3 different temperatures (i.e., 25 •C, 45 •C and 65 •C). A comparison of the DA function parameters obtained before and after adding recent data is shown in Table 3.

Table 3. A comparison of the DA function parameters before and after adding recent data to databank..

Radionuclide	$q_{equilibrium}^{maximum}$ (μmole/g MST)*		*E/R* (•C^{-1})*		*S* (μMolar)*		"*n*" Exponent*		$r^{\#}$	
	Before	After	Before	After	Before	After	Before	After	Before	After
Strontium	410±138	49±14	79±13	1333±256	0.42±.12	0.8±.01	.55±.33	2.5±.4	91	87
Plutonium	2.6±.5	2.55±1.1	8±6E-4	1771±312	0.8±1.2	3±1.7	2±1	4.2±.9	74	78
Uranium	1865±472	198±43	7±15E-9	19.4±1.9	68±.3	64±8	0.16±.01	0.2±.06	92	94
Neptunium	65±9	52±11	533±126	847±147	75.3±.01	92±7	1.1±.5	1.4±.03	90	95

* Parameters from equation 1
# Parameters from equation 7

An inspection of Table 3 shows a significant difference between the "before" and "after" parameters. Despite these differences, the collective action of these parameters to the DA function yielded the same fitting performance as reflected in the values of the correlation coefficient (*r*). Both expressions will predict the same loading and equilibrium concentrations.

Strontium

$$Loaded\ \underset{eq}{\mathrm{Sr}} = 49 \pm 4 \times e^{-\left(\frac{273 + \text{Temperature}}{1333}\right)^{2.5 \pm 0.3} \times \left(Ln\frac{0.8 \pm 0.01}{[Sr]}\right)^{2.5 \pm 0.3}} \quad 9$$

Plutonium

$$Loaded\ Pu_{eq} = 2.55 \pm 1.1 e^{-\left(\frac{Temperature + 273}{1771}\right)^{4.2 \pm 0.9} \times \left[Ln\frac{3 \pm 1.7}{[Pu]}\right]^{4.2 \pm 0.9}} \quad 10$$

Uranium

$$Loaded\ U_{eq} = 198 \pm 43 \times e^{-\left(\frac{Temperature + 273}{19.4}\right)^{0.2 \pm .06} \times \left(Ln\frac{64 \pm 8}{[U]}\right)^{0.2 \pm .06}} \quad 11$$

Neptunium

$$Loaded\ Np_{eq} = 52 \pm 11 \times e^{-\left(\frac{Temperature + 273}{847}\right)^{1.4 \pm .3} \times \left[Ln\frac{92 \pm 7}{[Np]}\right]^{1.4 \pm .3}} \quad 12$$

We re-fit the radionuclide loading data with temperature added as a variable in the DA function. Re-fitting Np data with temperature as a variable was not possible since the spread in the Np data was large. The resulting fitting DA functions are shown in Appendix B. Analysis of functions in Appendix B yielded the adsorption energy for each radionuclide on MST. The sorption energy for Pu, Sr and U measured 49 kJ/mole, 1.5e-4 and 4.5e-5 J/mole respectively.

3.2 Model Discrimination between the Kinetic Functions

Discrimination analysis focused on two nuclides, plutonium and uranium. Appendix C provides a summary table of the fitting results (Sum of Square Errors) for each of the sorbates. We prefer that a single kinetic function provide a good fit for all four sorbates. Visual inspection of Appendix C revealed that the 1st order, 2nd order and Diffusion-limited models exhibited large residual errors. The Rudzinski model was not further considered because of the large number of mathematical operations and sensitivity to coefficients variations. Although both the Elovich and Power function fitted the uranium data best, loading with these functions are never expected to reach steady state. Recall one function contains an exponent and the other a power of 10. The Pu loading data always reached steady state under several different initial conditions ruling out the Elovich and Power functions for fitting. Therefore, we excluded the Elovich and Power kinetic functions for further consideration.

The remaining two models, Rahn and Ritchie, had similar fitting performance. The Ritchie model is based on a number of surface sites, *n*, occupied by each radionuclide ion. Therefore, integration of the kinetic equation in Table 2 leads to the Ritchie function in Table 1. In the case of the Rahn's model, both adsorption on and transport to the MST surface control the rate of radionuclide adsorption. A mathematical description of the Rahn's model follows.

$$\frac{dq}{dt} = k \times \left(q_{eq} - q\right) \times D \frac{\partial C}{\partial X}; \quad \frac{\partial C}{\partial X} \propto f\left(C_{bulk}, D\right) \times t^{n} \quad for\ semi-infinite\ plane\ diffusion$$

$$\int_0^q \frac{dq}{\left(q_{eq} - q\right)} = \int_0^t k \times f\left(C_{bulk}, D\right) \times t^{n} dt \rightarrow \quad q = q_{eq} \times \left(1 - e^{\frac{k \times f\left(C_{bulk}, D\right) \times t^{n+1}}{n+1}}\right)$$

We also considered the behavior of the rate constants derived from both of these models with varying MST concentration and initial sorbate concentrations. We observed that the rate of sorbate loading (*dq/dt*) was the same under various different conditions as shown in Figures D1 to D4 in Appendix D. Since the rate of loading is proportional to the final equilibrium loading, the expression in equation 13 indicates that the rate constant should decrease with equilibrium loading.

$$\frac{dq}{dt} = k(\downarrow)\left(q_{\mathrm{eq}}(\uparrow) - q(t)\right) \qquad if\ q_{\mathrm{eq}}\ increases, k\ should\ decrease \qquad 13$$

Decreasing the MST concentration or increasing the sorbate concentration should decrease the rate constant. However, the rate constant should not change with loading capacity since it is a constant. Therefore, the data indicates that the rate of loading was controlled by diffusion to the MST (transport limited). Since both functions (Rahn and Ritchie) fit the loading data on MST, we chose the Rahn function for fitting this data since this function includes transport limited adsorption. It was also observed that the Pu rate constant data shown in Figures 2A (Rahn) and 2B (Ritchie) revealed a significant noise (including bifurcation behavior resulting from the mathematical form and

complexity) with the Ritchie's rate constant values, but not with the rate constant derived from the Rahn fitting function. Therefore, we selected the Rahn function to describe sorption on MST.

We fit the Rahn function to the sorption data of all radionuclides. A sample of the fitting performance of the Rahn function is shown in the figures included in Appendix E. A visual inspection of the figures in Appendix E shows the good fit between the Rahn function and the radionuclide sorption data on MST. From this fitting, the rate constant and exponent associated with the Rahn function were derived. We also computed the sensitivity of these two (rate constant and exponent value) parameters derived from the Rahn function. The sensitivity of the Rahn function to variations of its parameters is shown in Appendix F. The figures show the values of the parameters that minimized the Sum of Square Errors (SSE). The figures clearly show that values for the rate constant and the exponent away from the minimum will vary the SSE values significantly.

To predict sorption kinetics, we need to correlate the two parameters from Rahn's function (rate constant and exponent value) to the MST capacity for a given radionuclide. We fit Rahn's rate constant as an inverse function of the equilibrium loading for each nuclide. The resulting fitting curves and a table summarizing the data are shown in appendix G. The tabulated data from the fits shown in Appendix G are included Appendix H. A review of the figures in Appendix G showed the Sr and U fitting was poor – r^2 values of 0.60 and 0.64, respectively – relative to the fitting performance with the Pu and Np data (r^2 values of 0.85 and 0.7 respectively). However, the fitted function provides the information needed to predict sorbate loading. The final loading functions for all sorbates follows.

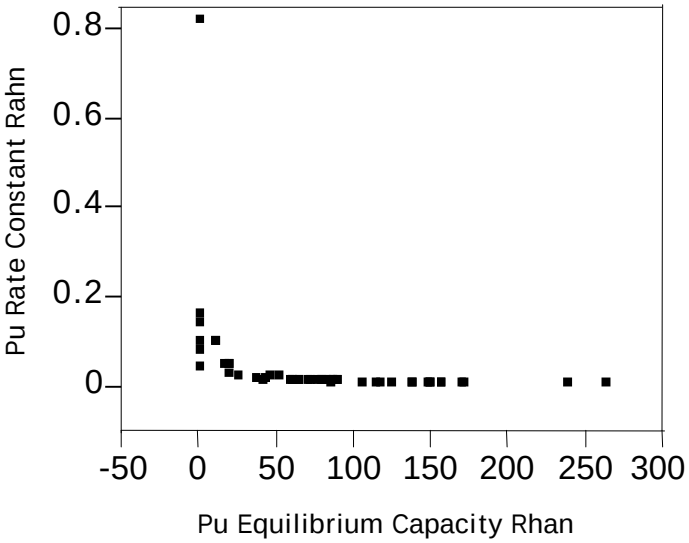

Figure 2A. The Pu rate constant as determine by the Rahn function

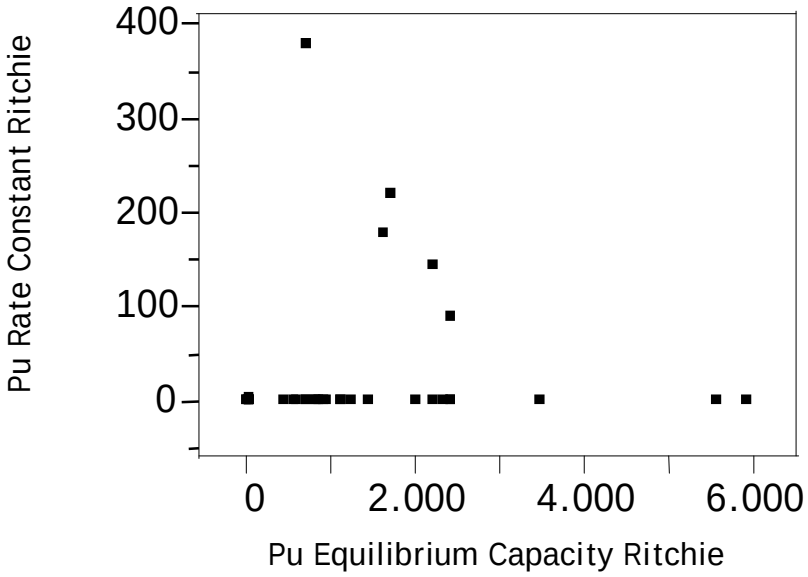

Figure 2B. The Pu rate constant as determined by the Ritchie function. Note the bifurcation in the data

3.3 Kinetic Functions

The Rahn kinetic function for the Pu loading data follows. Similar equations exist for the other sorbates.

$$q_{Pu}(t) = q_{Pu-eq} \times \left[1 - e^{-kt^n}\right] \qquad 14$$

In this expression, $q_{Pu}(t)$ is the amount of plutonium loaded on MST (in units of micromole per grams of MST). The expression "$q_{pu\text{-}eq}$" is the equilibrium amount of plutonium on MST. To include the effect of the equilibrium loading on the rate constant, we fit the rate constant and exponent from the Rahn function to the equilibrium capacity. The relationship between the rate constant, the exponent and the equilibrium loading for each sorbate follows.

Plutonium

$$k = \frac{0.207 \pm 0.4}{Loaded\ Pu_{\text{eq}}} + 0.01 \pm 0.002 \qquad 15$$

$$n = \frac{1.71 \pm 0.8}{Loaded\ Pu_{\text{eq}}} + 0.01 \pm 0.006 \qquad 16$$

Strontium

$$k = \frac{-0.086 \pm 0.06}{Loaded\ Sr_{eq}} + 4 \pm 0.6 \qquad 17$$

$$n = \frac{0.7 \pm 0.02}{Loaded\ Sr_{eq}} + 0.36 \pm 0.13 \qquad 18$$

Uranium

$$k = \frac{1 \pm 0.34}{Loaded\ U_{eq}} + 0.16 \pm 0.1 \qquad 19$$

$$n = \frac{0.7 \pm 0.4}{Loaded\ U_{eq}} + 0.36 \pm 0.07 \qquad 20$$

Neptunium

$$k = \frac{2.1 \pm 0.4}{Loaded\ Np_{eq}} + 0.11 \pm 0.12 \qquad 21$$

$$n = \frac{-0.26 \pm 0.1}{Loaded\ Np_{eq}} + 0.55 \pm 0.3 \qquad 22$$

3.4 Model Validation

We calculated the radionuclide sorption on MST at a concentration of 0.4 g/L and at 25 •C. The starting radionuclide concentrations and conditions for this prediction were identical to the experimental data obtained in previous report.[15] Please note the data set in that report was not considered during the formulation of the current isotherm model. A comparison of plutonium, uranium and neptunium loading with predictions is shown in Figures 3A, 3B and 3C.

An inspection of Figures 3A, 3B and 3C showed that the model over-predicts neptunium sorption but under-predicts plutonium and uranium sorption data. In the case of uranium, the data did not reach equilibrium in 30 hours of testing. Therefore, the precision of the model's predictions cannot be fully ascertained.

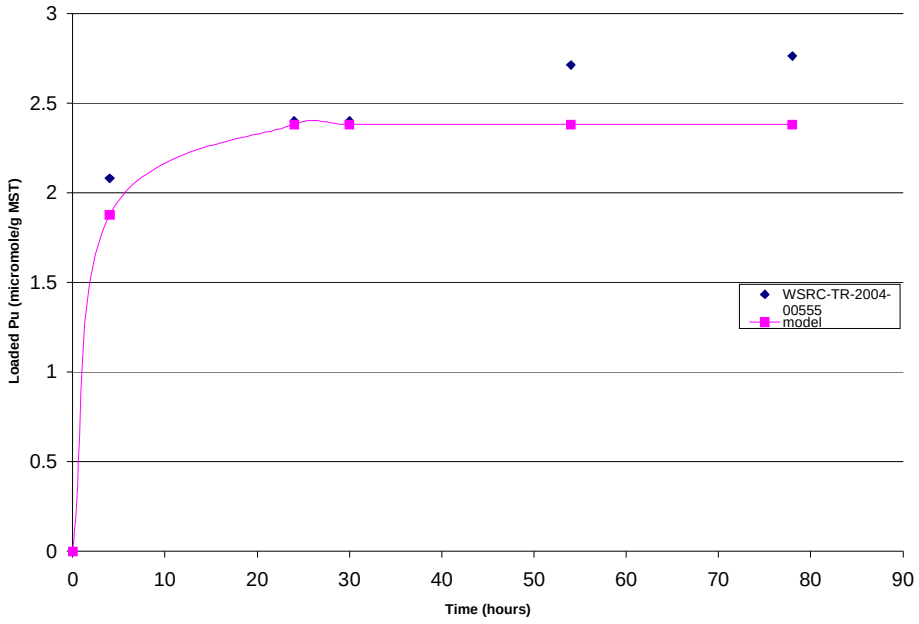

Figure 3A. Comparison of the plutonium loading on MST from Table 2 in Ref.14 and the model's predictions.

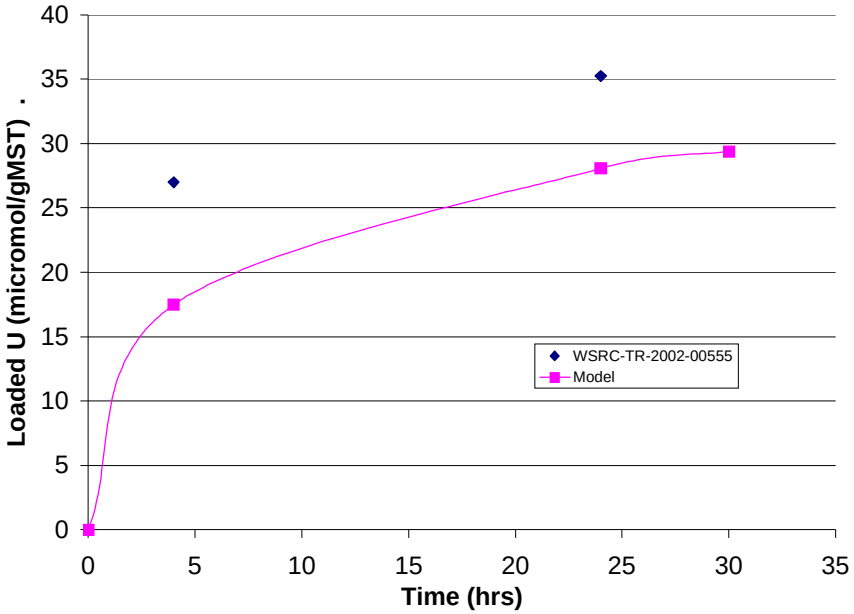

Figure 3B. Comparison of the uranium loading on MST from Ref. 14

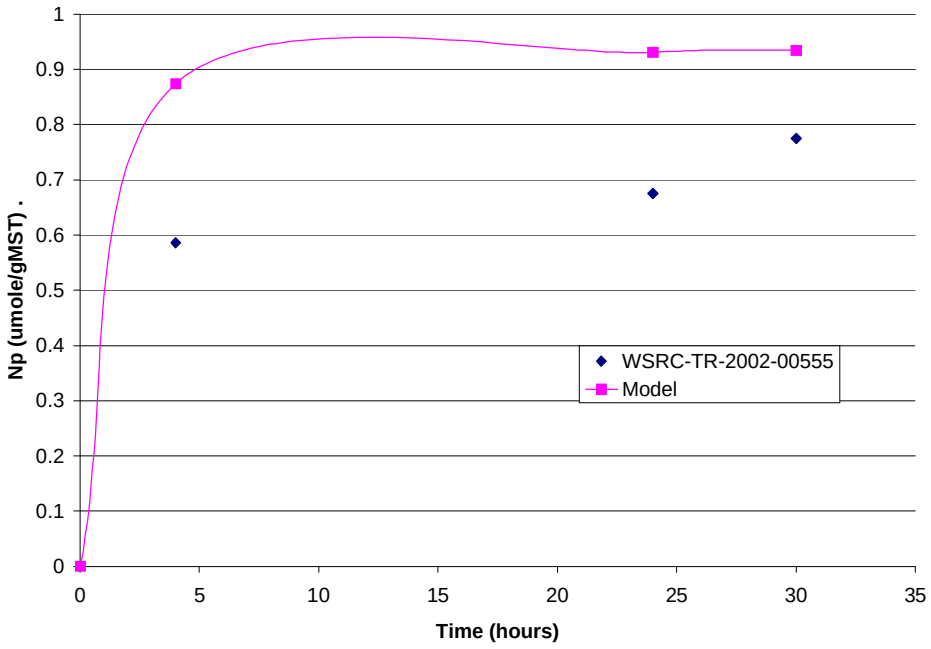

Figure 3C. Comparison of the neptunium loading on MST from Ref. 14 and the model's predictions.

3.5 Calculation Example

Decontamination Factor Calculation

Consider a waste solution initially containing 1.15 • M (0.3 mg/L) Pu is to be mix for 4 hours with 0.4 g/L MST. These conditions are identical to those tested in Ref. 15. First, we must determine the equilibrium amount of Pu loaded on MST. This is done by simultaneously solving equations 1 and 2. We plotted equations 1 and 2 in Figure 4. The intersection of the curve and the line provides the equilibrium amount of Pu on MST. Inspection of Figure 4 shows the equilibrium amount of Pu on MST is 2.38 • moles/g of MST. We substituted this value into the Rahn function (listed in Table 1) and solved for the amount of Pu loaded on MST after 4 hours of mixing. The loaded amount calculated to be 1.877 • moles/g of MST. This value was substituted into equation 2 and we solved for the concentration of Pu in solution. We obtained a concentration of 0.55 • Molar. The corresponding decontamination factor is 2. The DF value reported after 4 hours of test in Ref. 15 is 3.7. This shows the model under-predicts Pu loading on MST.

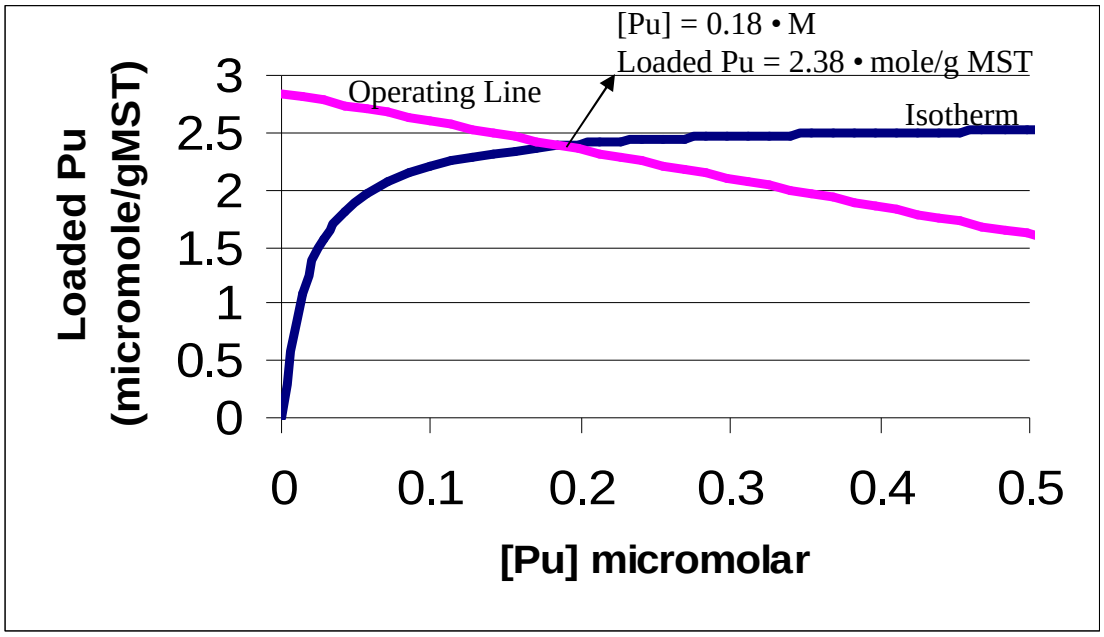

Figure 4. The intersection of the operating line, determined by a solution containing 1.15 • M Pu and 0.4 g/L MST, and the Pu Isotherm curve.

3.6 Temperature Effect

The expanded data set contained sorption data at three different temperatures (i.e., 25, 45 and 65 •C). We plotted the rate constant of radionuclide sorption on MST as a function of temperature. Figures 5A, 5B, 5C and 5D provide plots of the rate constants as a function of temperature for Pu, Sr, U and Np, respectively. We fit the "modified" Arrhenius function[16] shown in equation 23 to Figures 5A, 5B, 5C and 5D. The results of the fit are represented by the solid line curve going through the data in each figure. The mathematical function in each figure represents the best fit to the data. A closer inspection of Figures 5A and 5B shows that the rate constant from the Pu and Sr sorption data did not obey the Arrhenius function. In these two cases, we used the average rate constant over the temperature range studied. The average rate constant was 0.0263 and 3.57 (1/(• mole Pu per g of MST*hr)) for Pu and Sr respectively. On the other hand, U and Np rate constants obey the "general" Arrhenius function as shown in the close fit between the solid line and the data in Figures 5C and 5D. The calculated activation energy for sorption on MST was 19 and 10.3 kJ/mole for U and Np respectively. This energy is within the activation energy of ion diffusion in water reported to be 15 to 30 kJ/mole.[17,18] Therefore, the measured radionuclide sorption on MST is transport controlled. Although sufficient mixing can in theory increase radionuclide transport through the boundary layer around MST, the range of available mixing speed in facility design is likely not sufficient to overcome radionuclide diffusion in solution as observed in the laboratory experiments. Laboratory studies examined a relatively wide range of mixing energies that incorporate those planned for the Actinide Removal Process and likely approach those for the Salt Waste Processing Facility.

$$k = k_o \times T^n \times e^{-\frac{\Delta E}{RT}} \qquad 23$$

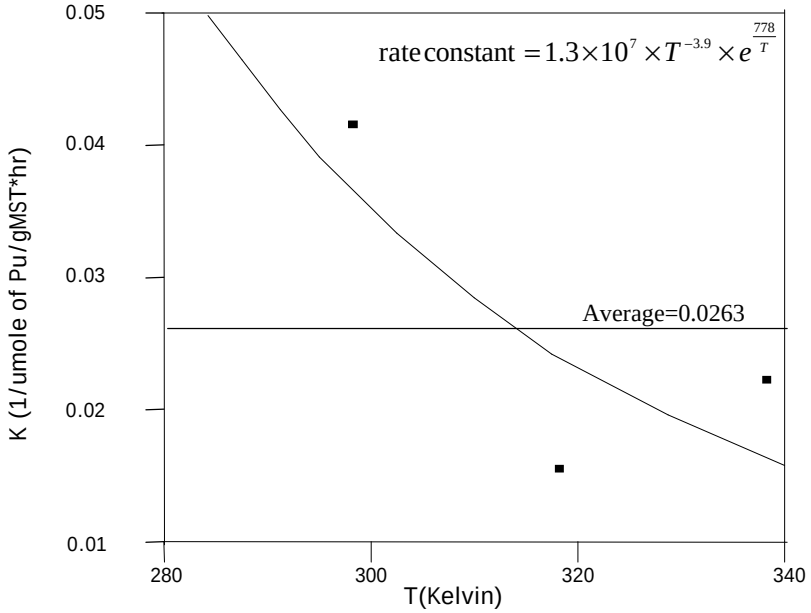

Figure 5A. The Rahn function rate constant as a function of temperature for the Pu sorption.

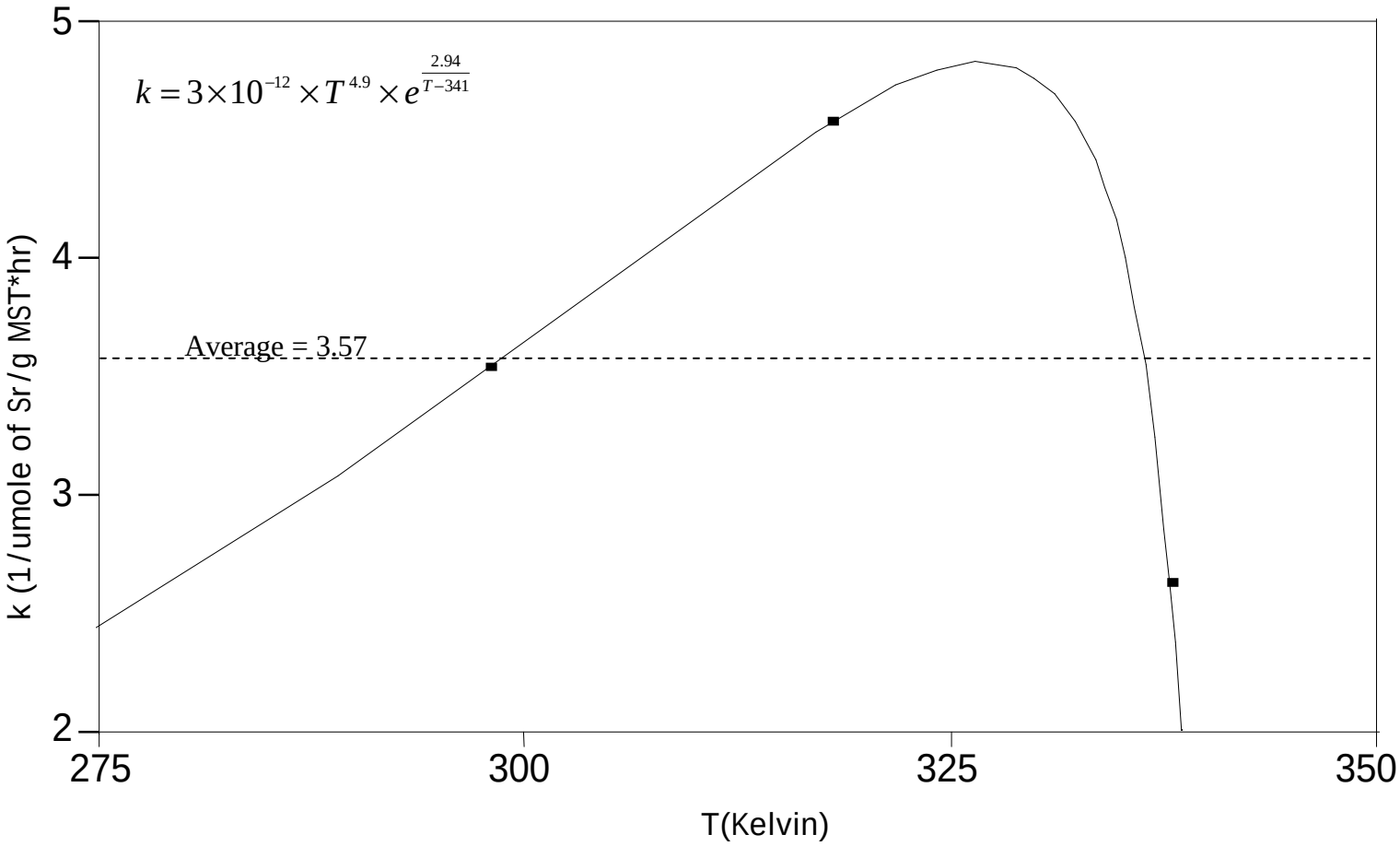

Figure 5B. The rate constant as a function of temperature for Sr sorption on MST.

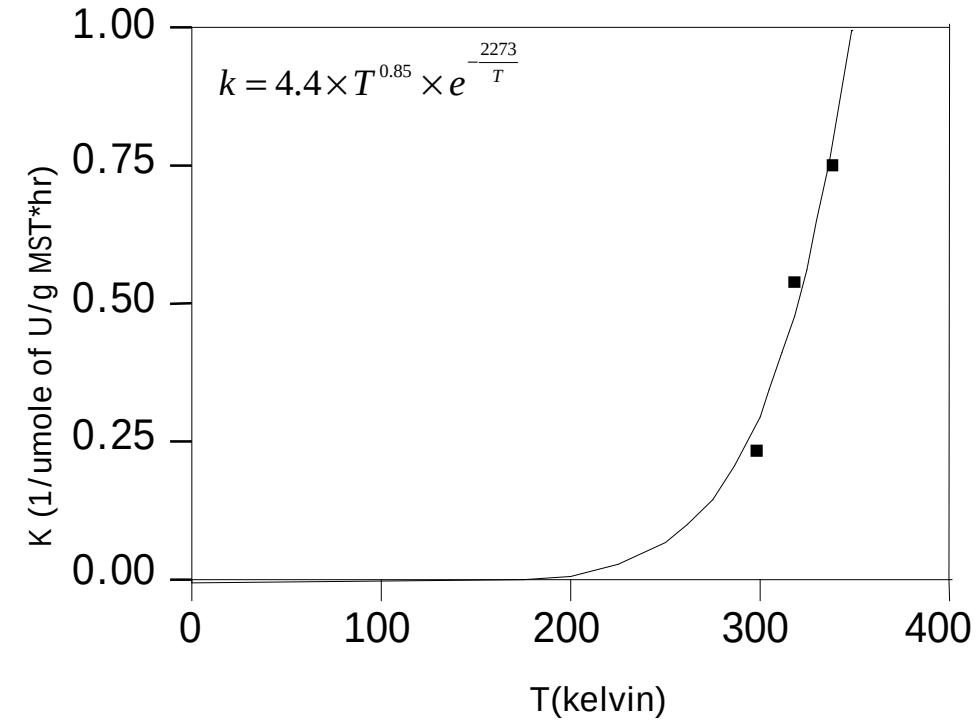

Figure 5C. The rate constant of U sorption on MST as a function of temperature.

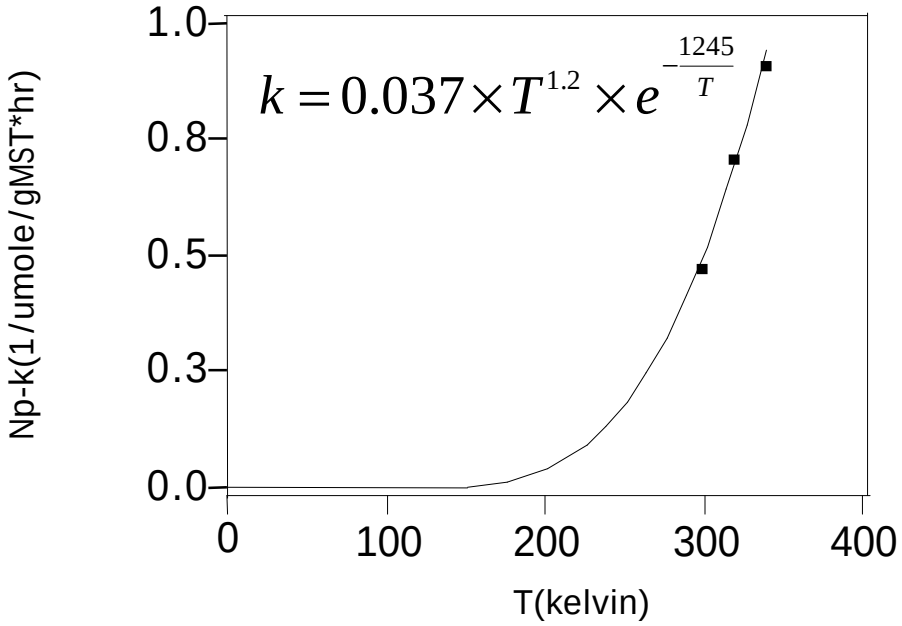

Figure 5D. The rate constant of Np sorption on MST as a function of temperature.

4.0 Conclusions

The DA isotherm parameters for U, Pu, Sr and Np have been updated to include additional data obtained since the original derivation. The DA isotherms were modified to include a kinetic function derived by Rahn to describe sorbate loading from the beginning of sorption up to equilibrium. The final functions describe both kinetic and thermodynamic sorption. We selected the Rahn function to describe radionuclide sorption because it originates from diffusion and absorption controlled sorption. An investigation of the thermal behavior of radionuclide sorption on MST as shown by this data revealed the sorption process is diffusion (or transport) controlled (in solution). Transport in solution can in theory be accelerated by vigorous mixing but the range of available mixing speed in the facility design will probably not be sufficient to markedly increase radionuclide sorption rate on MST from diffusion-controlled sorption.[19] The laboratory studies included mixing energies hydraulically-scaled to match those of the Actinide Removal Process and these likely approximate the range of energies available in the Salt Waste Processing Facility.

Appendix A:
Dubinin-Astashov Fitting of Strontium and the Actinides.

In these figures, data shown in open circle is from the latest radionuclide sorption test. Filled squares are from Phase 3 & 4 sorption tests. Phase 3 and 4 data is from:1) D. T. Hobbs, M. G. Bronikowski, T. B. Edwards, and R. L. Pulmano, "Final Report of Phase III Testing of Mono-Na Titanate Adsorption Kinetics," WSRC-TR-99-00134, Rev. 0, May 28,, 1999, 2) D. T. Hobbs, and R. L. Pulmano, "Phase IV Simulant Testing of Mono-Na Titanate Adsorption Kinetics", WSRC-TR-99-00219, Rev. 0, June 29, 1999, and 3) D. T. Hobbs, "Phase V Simulant Testing of Monosodium Titanate Adsorption", WSRC-TR-2000-00142, Rev. 0, May 22, 2000.

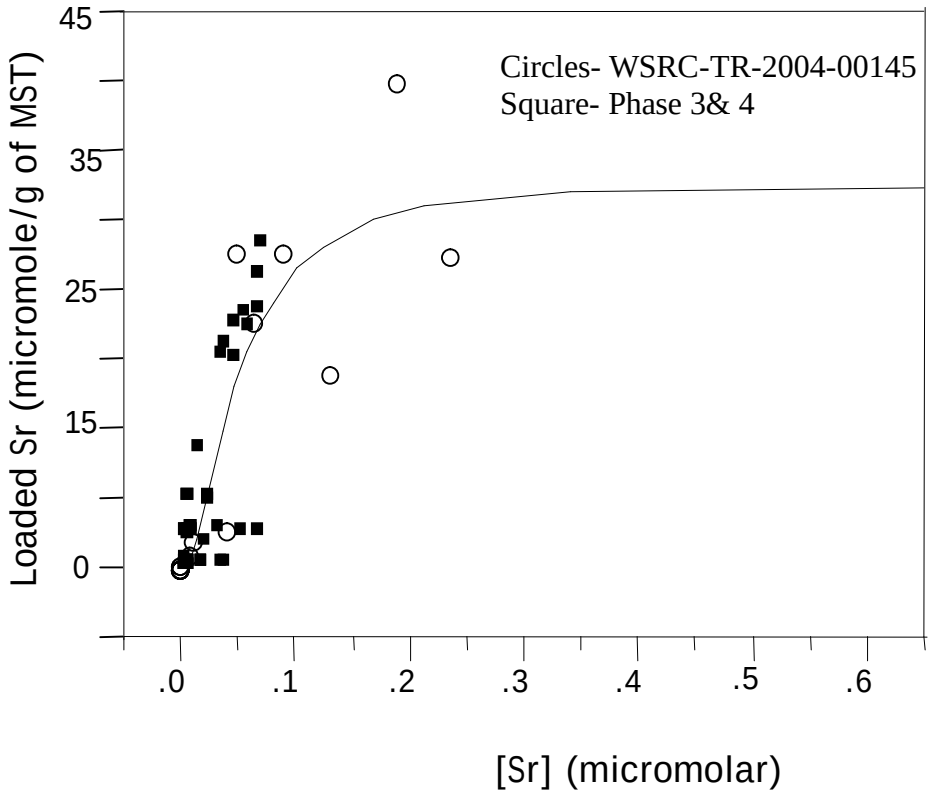

Figure A1. The DA function fitting of the Sr loading curve. Circles from M. J. Barnes et al. 'Monosodium Titanate Multi-strike Testing,' WSRC-TR-2004-00145, Rev. 0, April 2004.

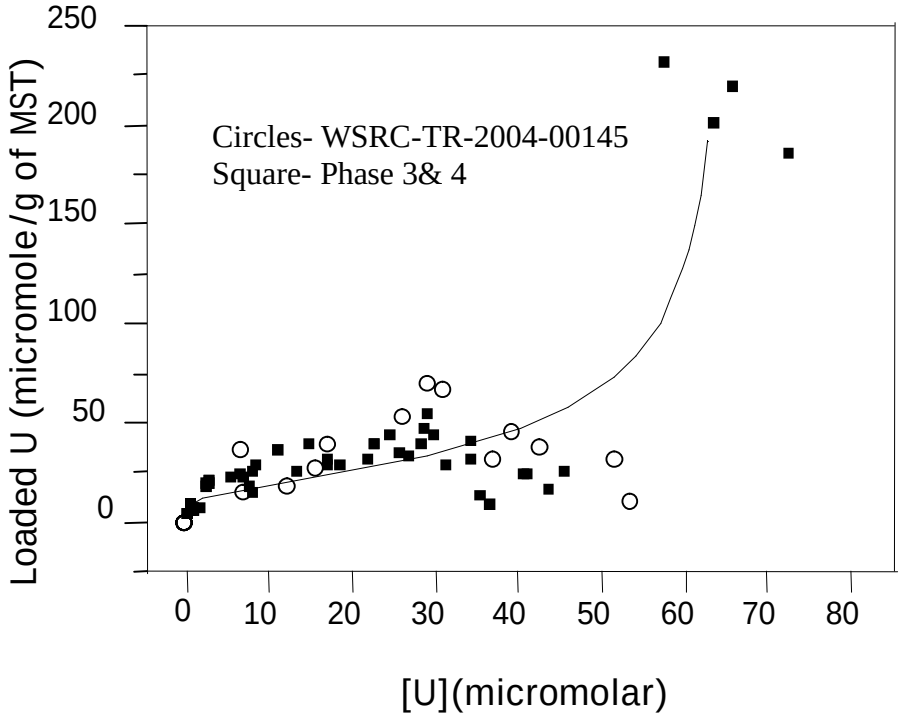

Figure A2. The DA function fitting of U loading data. Circles from M. J. Barnes et al. 'Monosodium Titanate Multi-strike Testing,' WSRC-TR-2004-00145, Rev. 0, April 2004.

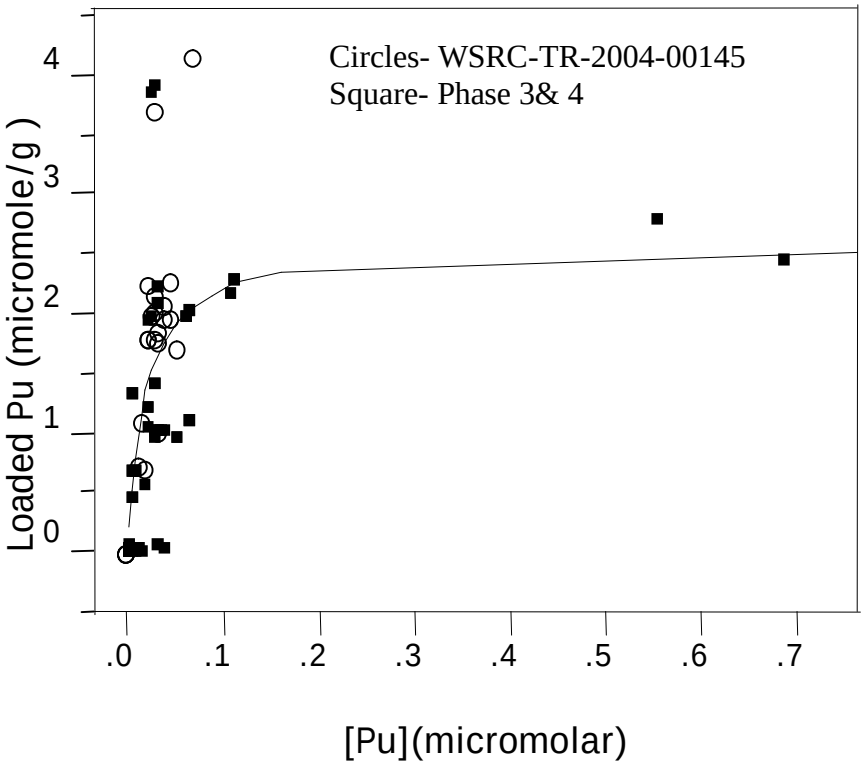

Figure A3. The DA function fitting of the Pu loading data. Circles from M. J. Barnes et al. 'Monosodium Titanate Multi-strike Testing,' WSRC-TR-2004-00145, Rev. 0, April 2004.

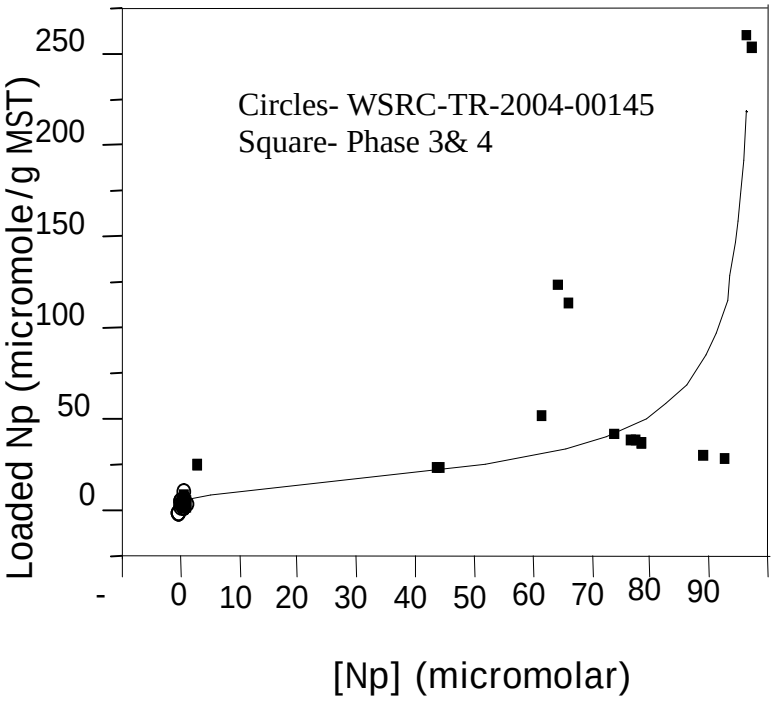

Figure A4. DA function fitting of the Np loading data. Circles from M. J. Barnes et al. 'Monosodium Titanate Multi-strike Testing,' WSRC-TR-2004-00145, Rev. 0, April 2004.

Appendix B

The Dubinin-Astashov function fitting of the radionuclide database with temperature as a variable. The coefficient before the temperature variable is equal to the R/E where R stand for the gas constant (8.314 J/mole •C) and E stands for the sorption energy (J/mole).

$$Loaded\ Pu = 3.26 \times e^{-\left[0.00017 \times (T+273) \times Ln\left(\frac{1.2E7}{[Pu]}\right)\right]^{9.2}}$$

$$Loaded\ Sr = 223.6 \times e^{-\left[54245 \times (T+237) \times Ln\left(\frac{1.2e10}{[Sr]}\right)\right]^{5.78}}$$

$$Loaded\ U = 15112 \times e^{-\left[186322 \times (T+273) \times Ln\left(\frac{68.15}{[U]}\right)\right]^{0.1}}$$

For Np, three equations are shown for the different temperatures obtained

At $25°C$

$$110830 \times e^{-\left[1.4e8 \times Ln\left(\frac{92.4}{[Np]}\right)\right]^{0.11}}$$

At $45°C$

$$93.1 \times e^{-\left[79.5 \times Ln\left(\frac{60}{[Np]}\right)\right]^{2.2}}$$

At $65°C$

$$708118 \times e^{-\left[36.84 \times Ln\left(\frac{816}{[Np]}\right)\right]^{0.43}}$$

Appendix C. Sum of Square Error (SSE) values for the kinetic models

Table C1. Sum of Square Error (SSE) values for the kinetic models

Actinide	Initial concentration (μM)	MST (g/L)	1st Order	2nd Order	Elovich	Rahn	Ritchie	Power	Diffusion	Rudzinski
Pu	0.0047	0.2	1.07	0.95	0.14	0.16	0.16	0.18	4.5	0.19
Pu	0.0047	2	1.13	1.04	0.94	0.92	0.96	0.94	2.6	0.95
Pu	0.04	0.2	0.88	0.81	1.02	.48	0.33	1.1	5.6	0.24
Pu	0.04	2	0.91	0.78	0.93	0.28	0.23	1.04	5.4	0.25
Pu	1.17	0.2	1.24	1.33	1.48	0.32	0.26	1.65	7.0	0.31
Pu	1.17	2	1.2	1.02	1.43	0.37	0.73	1.48	6.3	0.53
Pu	0.7	0.2	1.0	0.32	0.438	0.84	0.48	.62	-	0.35
Pu	0.7	2	1.1	0.42	0.24	0.92	0.12	.36	-	0.09
Pu	0.27	0.4	0.92	0.9	0.73	0.82	0.69	1.2	5.2	0.89
Pu	0.27	0.4	1.0	0.94	0.82	0.78	0.86	1.25	4.9	0.91
Pu	0.8	0.4	1.4	0.99	0.94	0.92	1.1	1.16	6.8	0.77
Pu	0.8	0.4	1.2	1.1	0.95	0.96	0.92	1.0	6.2	0.76
Pu	0.92	0.4	1.7	1.4	0.96	0.90	0.95	1.4	7.4	0.83
Pu	0.85	0.4	1.6	1.7	0.96	0.95	0.88	1.37	6.8	0.66
Pu	0.41	0.4	1.3	1.3	0.92	0.88	0.84	1.43	4.45	0.58
Pu	0.43	0.4	1.4	1.45	0.86	0.83	0.90	1.88	4.9	0.64
Pu	0.43	0.4	2.1	1.8	0.84	0.81	0.80	1.91	5.2	0.69
Pu	0.43	0.4	1.7	1.66	0.94	0.91	0.89	1.68	4.2	0.55
Pu	0.43	0.4	1.3	1.23	0.85	0.85	0.83	1.32	4.6	0.61

Actinide	Initial concentration (μM)	MST (g/L)	1st Order	2nd Order	Elovich	Rahn	Ritchie	Power	Diffusion	Rudzinski
U	103	0.2	239	323	12	243	85	14	1044	78
U	103	2	247	289	27	432	34	24	-	46
U	62	0.2	122	341	16	428	63	15	-	55
U	62	2	113	419	18	238	47	21	-	46
U	38	0.2	44	410	38	298	38	48	-	48
U	38	2	47	344	42	308	77	39	-	77
U	37.9	0.4	111	165	34	347	111	79	661	53
U	37.9	0.4	151	86	37	276	65	54	9004	40
U	39.4	0.4	127	151	47	246	87	46	123	23
U	38.8	0.4	199	153	39	248	92	42	472	86
U	46.2	0.4	128	113	27	326	90	44	9782	74
U	41.9	0.4	136	113	47	316	70	39	5041	20
U	55.4	0.4	121	88	64	382	139	114	9222	71
U	49.9	0.4	103	91	57	253	139	45	8255	96
U	49.9	0.4	199	80	85	243	109	68	5304	70
U	49.9	0.4	170	114	94	273	60	70	6392	45
U	49.9	0.4	178	79	74	228	76	44	6788	33
U	49.9	0.4	154	81	34	212	148	109	8866	23
U	29.6	0.4	115	116	57	271	88	92	3284	24
U	33.9	0.4	173	156	38	236	155	129	8724	70
U	25.0	0.4	114	143	48	248	89	50	9882	36
U	29.9	0.4	190	149	47	273	119	64	7551	49
U	18.9	0.4	130	134	56	284	127	112	3187	61

U	23.1	0.4	116	89	64	299	114	103	6095	66
U	43.7	0.4	175	89	56	281	111	36	6096	53
U	18.2	0.4	115	158	64	267	110	42	6125	48
U	27.8	0.4	159	147	45	315	157	73	8348	92
U	29.3	0.4	192	74	55	318	141	116	2174	33
Actinide	Initial concentration (µM)	MST (g/L)	1^{st} Order	2^{nd} Order	Elovich	Rahn	Ritchie	Power	Diffusion	Rudzinski
Sr	0.6	0.2	0.74	0.65	0.57	.63	.14	.46	23	.11
Sr	0.6	2	0.81	0.78	0.78	.78	.80	1.4	-	.84
Sr	0.093	0.2	0.35	0.23	0.423	.30	.22	.61	-	.33
Sr	0.093	2	0.49	0.24	0.43	.44	.20	.72	-	.23
Sr	0.71	0.2	0.89	1.45	0.98	.56	1.34	.83	-	1.29
Sr	0.71	2	0.76	1.91	0.84	.38	1.88	.79	-	1.67
Sr	1.01	0.2	1.21	0.983	1.25	0.89	.878	1.14	-	.9
Sr	1.01	2	1.34	0.824	0.825	0.68	.674	.91	-	.66
Sr	1.2	0.2	1.95	1.28	1.354	1.1	1.1	1.24	-	.95
Sr	1.2	2	1.9	1.44	3.49	1.29	1.12	2.78	-	1.2
Sr	1.0	0.4	1.39	0.99	0.85	0.57	0.60	0.64	0.71	1.19
Sr	1.0	0.4	1.10	0.97	0.57	0.45	1.09	0.95	0.89	1.00
Sr	1.0	0.4	0.86	0.91	0.70	0.48	0.67	1.31	0.76	0.70
Sr	1.0	0.4	0.98	0.93	0.77	0.47	1.14	1.39	0.87	0.74
Sr	1.1	0.4	0.94	0.87	0.65	0.58	0.79	1.35	0.93	0.97
Sr	1.0	0.4	0.85	0.98	0.61	0.63	1.00	1.14	0.79	0.83
Sr	0.7	0.4	0.99	1.03	0.94	0.73	0.89	1.13	1.09	0.81
Sr	1.1	0.4	1.38	0.75	0.69	0.81	1.00	0.68	0.72	0.62

Sr	1.1	0.4	0.87	0.94	0.78	0.87	0.90	1.01	0.97	0.93
Sr	1.1	0.4	1.24	0.57	0.62	0.77	0.83	0.86	1.07	0.89
Sr	1.1	0.4	0.91	1.01	0.76	0.57	1.06	0.91	0.98	0.91
Sr	1.1	0.4	1.05	0.50	0.84	0.83	0.96	0.89	0.96	0.99
Sr	7.1	0.4	1.48	0.93	0.53	0.91	0.79	1.08	0.88	0.95
Sr	7.5	0.4	1.41	0.73	0.93	0.93	0.78	0.95	0.92	0.79
Sr	3.5	0.4	1.36	0.56	0.89	0.75	0.95	0.93	0.90	1.29
Sr	6.2	0.4	0.80	0.89	0.92	0.88	0.97	0.96	0.85	0.45
Sr	6.2	0.4	0.90	0.86	0.98	0.84	0.91	0.81	0.77	0.39
Sr	9.5	0.4	1.25	0.96	0.86	0.93	0.95	0.96	0.82	1.10
Sr	8.5	0.4	1.09	0.50	0.99	0.94	0.94	1.10	1.05	0.94
Sr	6.5	0.4	1.13	0.93	0.59	0.73	1.09	0.93	0.91	0.29
Sr	7.1	0.4	1.30	0.92	0.93	0.85	0.86	0.96	1.01	1.02
Sr	7.5	0.4	0.94	0.89	0.94	0.99	0.77	0.91	1.05	0.52
Actinide	Initial concentration (µM)	MST (g/L)	1^{st} Order	2^{nd} Order	Elovich	Rahn	Ritchie	Power	Diffusion	Rudzinski
Np	1.43	0.2	154	141	84	53	69	95	638	56
Np	1.43	2	198	134	184	143	79	168	-	79
Np	1.7	0.2	391	238	384	423	189	346	-	1787
Np	1.7	2	320	482	138	1032	328	147	-	330
Np	7.16	0.2	560	382	304	231	310	289	-	310
Np	7.16	2	501	427	348	487	419	329	-	411
Np	88.6	0.2	667	592	139	382	490	129	-	485
Np	88.6	2	495	236	354	428	200	388	-	198
Np	148	0.2	799	209	323	389	189	379	-	188

Np	148	2	813	1043	248	284	940	289	-	946
Np	1.7	0.4	447	254	367	261	154	239	685	940
Np	1.7	0.4	619	502	442	419	498	464	708	787
Np	1.8	0.4	777	488	660	370	477	617	405	650
Np	1.7	0.4	374	383	508	535	392	757	373	561
Np	1.9	0.4	462	494	637	405	406	317	617	924
Np	2.7	0.4	246	560	398	394	255	775	399	561
Np	2.2	0.4	616	638	407	479	470	943	673	368
Np	2.1	0.4	481	497	423	474	460	246	681	775
Np	2.1	0.4	314	628	690	804	354	531	683	514
Np	2.1	0.4	592	782	787	353	254	618	618	728
Np	2.1	0.4	647	888	506	427	487	891	303	444
Np	2.1	0.4	264	283	340	446	334	858	930	526
Np	1.0	0.4	328	232	457	455	240	413	820	551
Np	1.0	0.4	254	444	468	371	228	408	634	658
Np	1.0	0.4	736	248	344	688	344	363	539	421
Np	1.1	0.4	332	773	293	631	259	563	891	660
Np	1.1	0.4	456	377	503	404	451	504	685	622
Np	0.8	0.4	465	591	340	203	335	542	588	500
Np	1.3	0.4	204	510	593	423	453	458	589	663
Np	0.9	0.4	539	607	838	556	414	480	319	645
Np	0.9	0.4	784	595	293	287	272	615	646	636
Np	0.9	0.4	551	441	649	285	248	821	797	913

Appendix D. The effect of the initial radionuclide concentration on radionuclide sorption. The figures show results from duplicate experiments. Lines through the data are provided for visual aid. The point of these figures is to show that all the curves have the same initial slope independent of the initial radionuclide concentration. The data in these figures are from :1) D. T. Hobbs, M. G. Bronikowski, T. B. Edwards, and R. L. Pulmano, "Final Report of Phase III Testing of Mono-Na Titanate Adsorption Kinetics," WSRC-TR-99-00134, Rev. 0, May 28,, 1999, 2) D. T. Hobbs, and R. L. Pulmano, "Phase IV Simulant Testing of Mono-Na Titanate Adsorption Kinetics", WSRC-TR-99-00219, Rev. 0, June 29, 1999, and 3) D. T. Hobbs, "Phase V Simulant Testing of Monosodium Titanate Adsorption", WSRC-TR-2000-00142, Rev. 0, May 22, 2000.

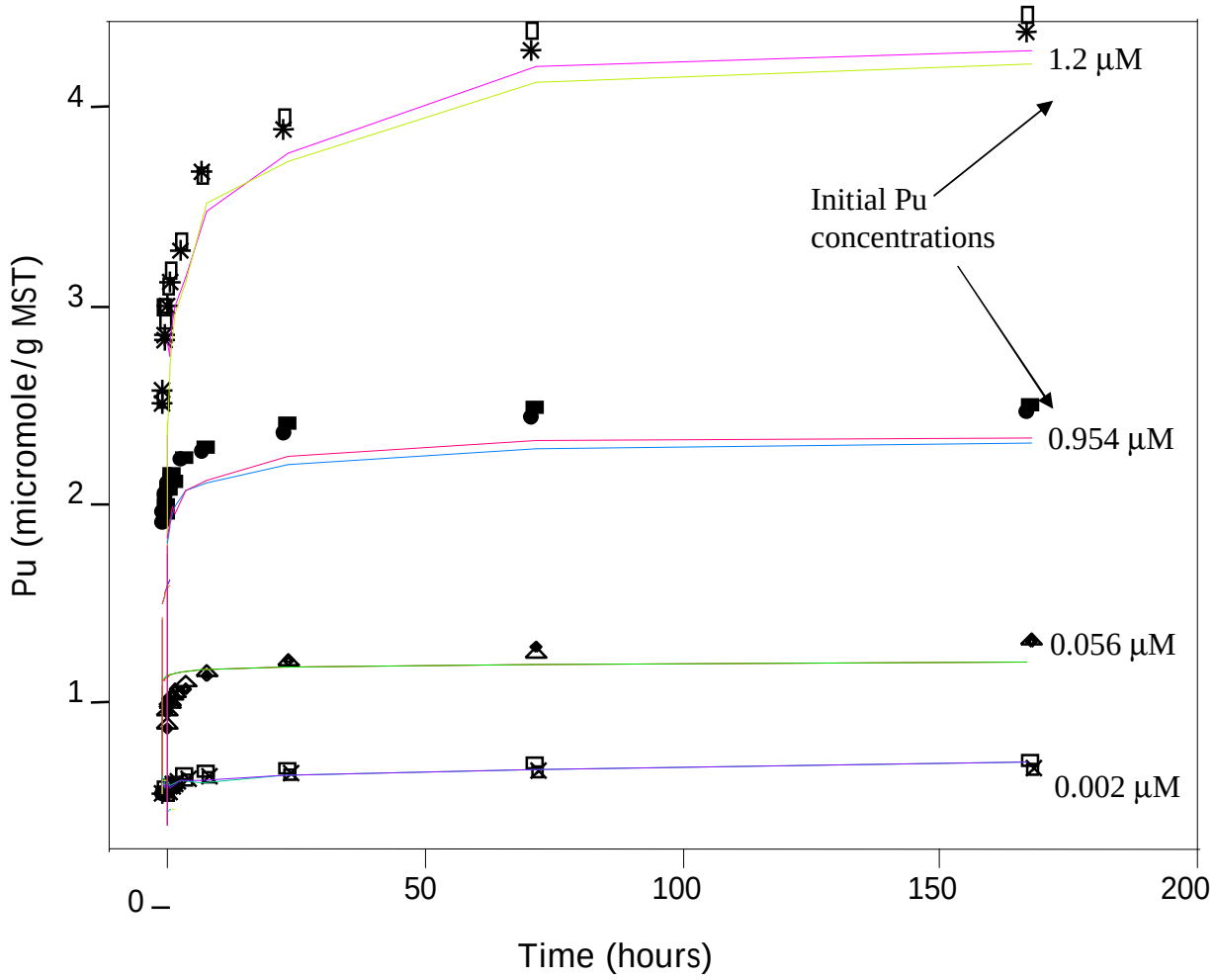

Figure D1. Loading curve for Pu on MST at different initial [Pu]. Note all curves have the same initial slope or rate of loading.

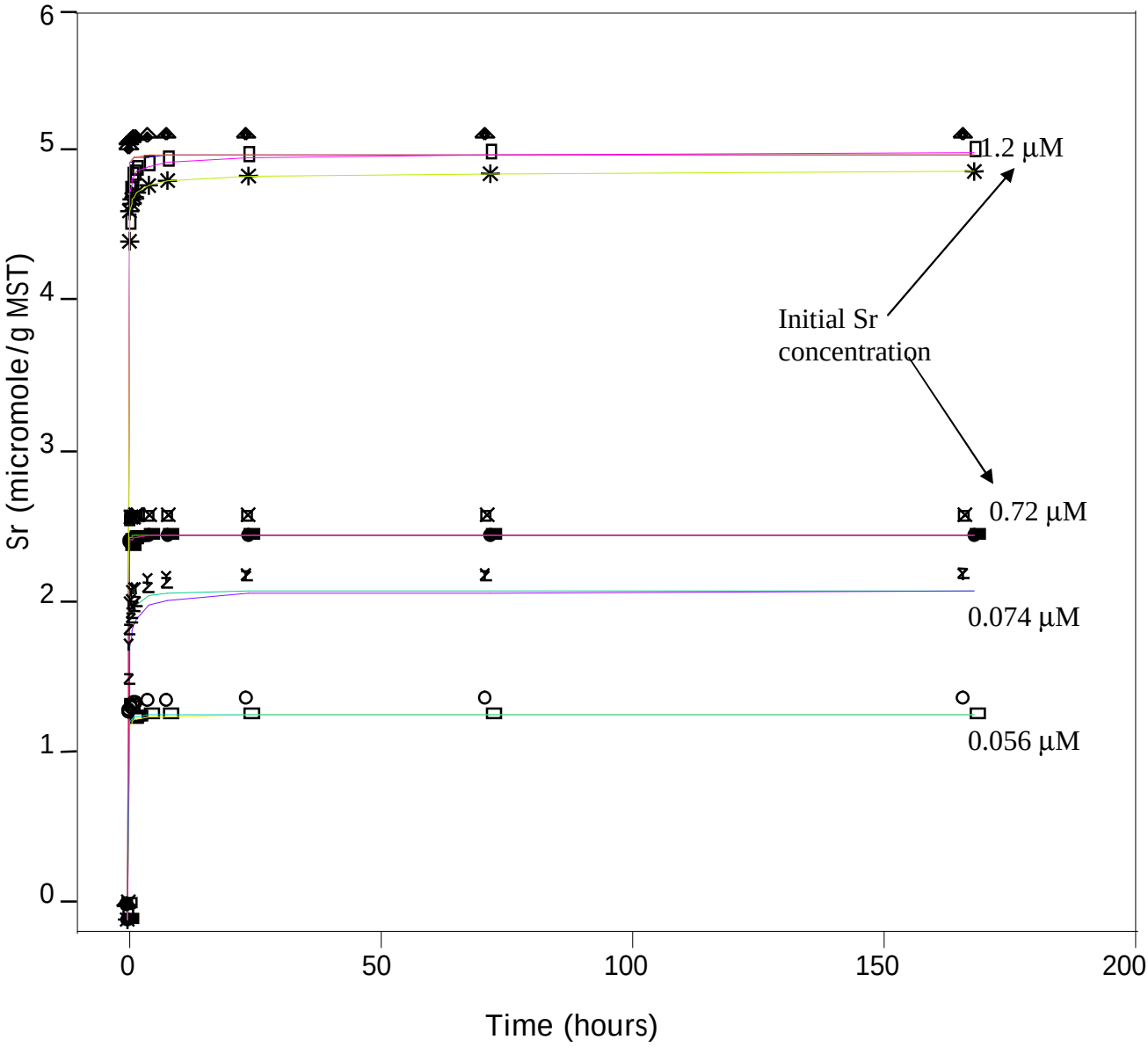

Figure D2. The loading curves of Sr on MST under various conditions. Note identical initial slope for all the curves.

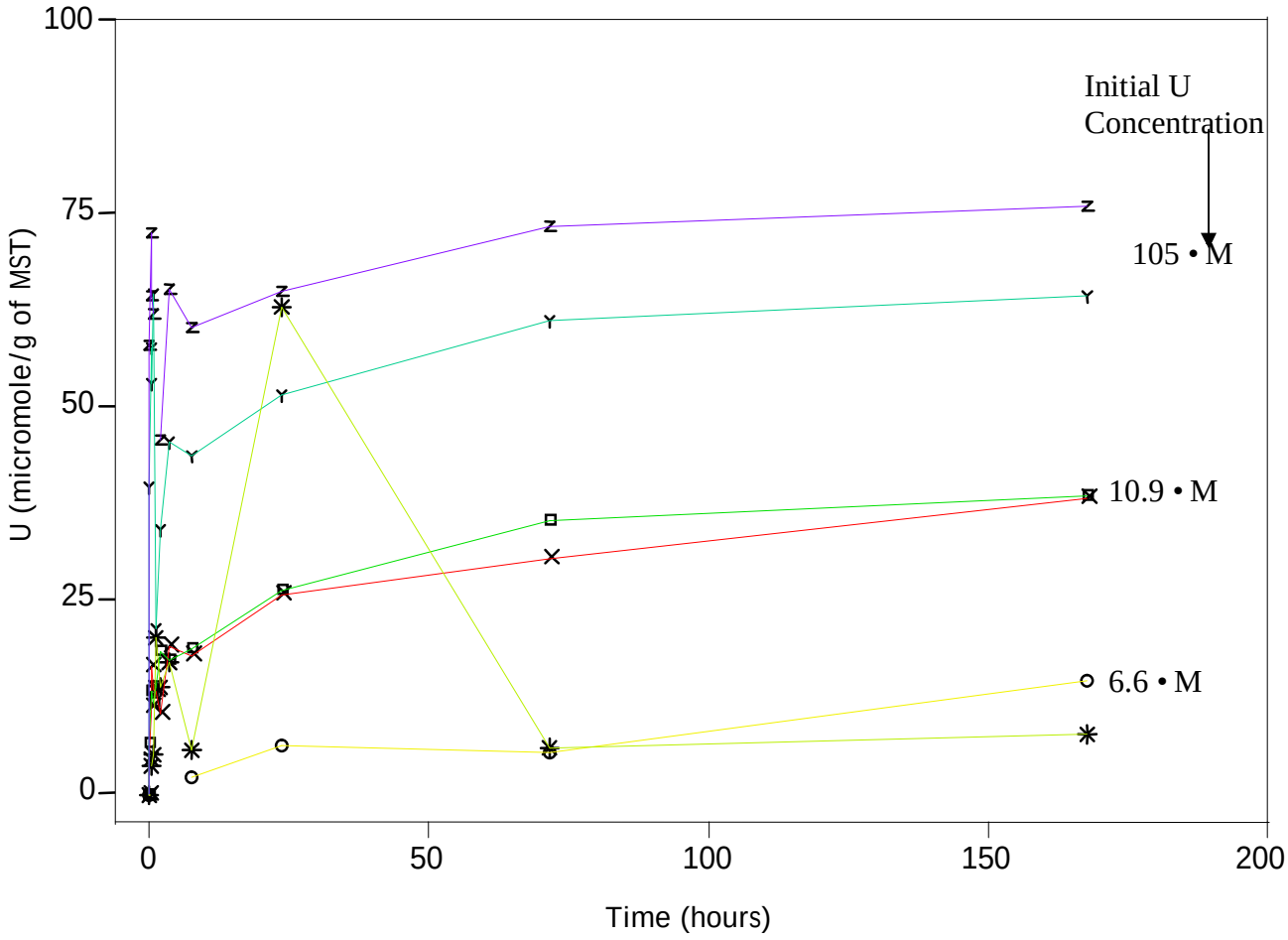

Figure D3. Loading curves of U at different initial [U] concentrations.

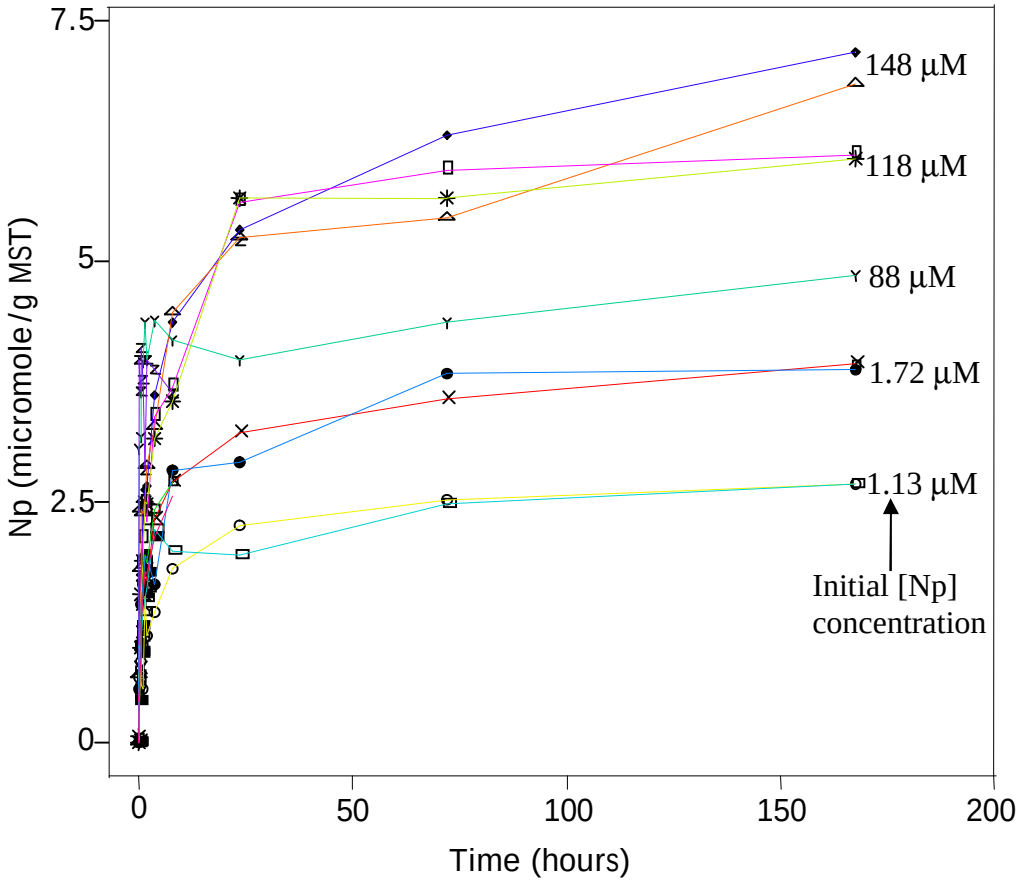

Figure D4. The loading curves of Np on MST at different initial [Np] concentrations.

Appendix E: Rahn's function fitting of the radionuclide sorption on MST under various conditions.

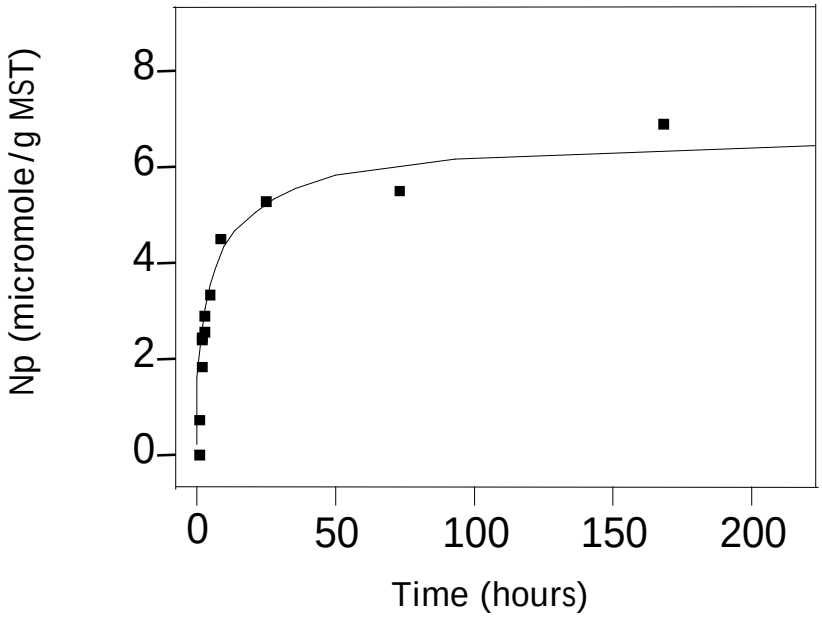

Figure E1. Np loading on MST at [OH]=1.43M,[Na]=6M ,T=25•C and g/L=0.2

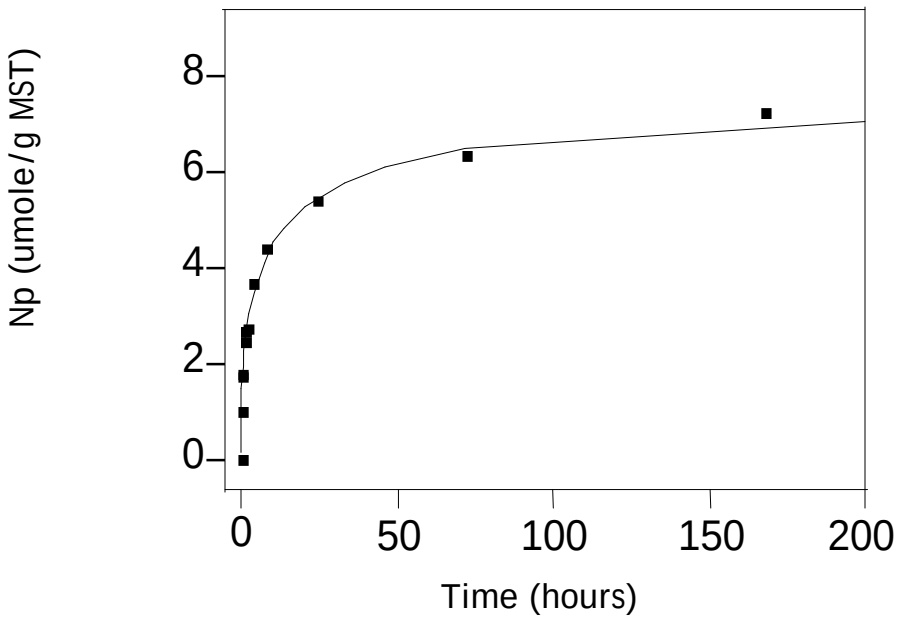

Figure E2. Np loading on MST at [OH]=1.43M,[Na]=6M, T=25•C and g/L =1.1.

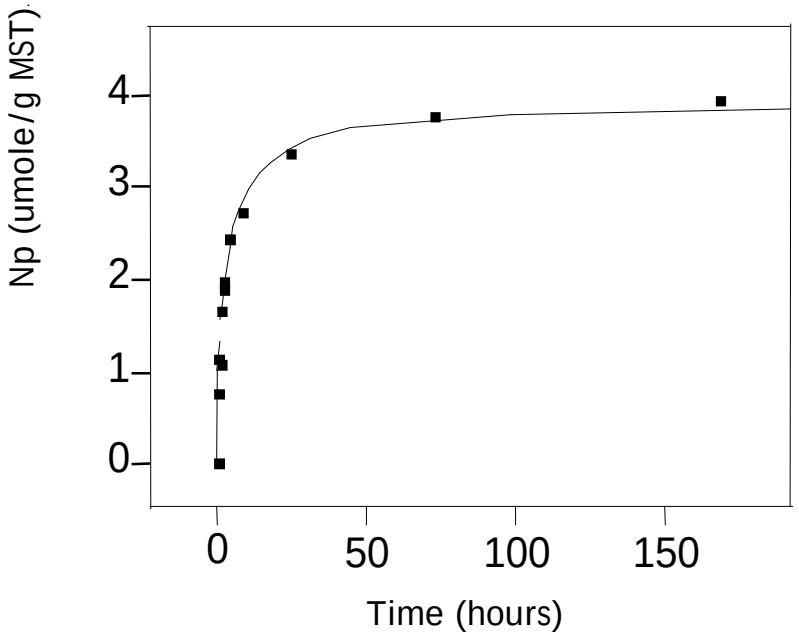

Figure E3. Np loading on MST at [OH]=1M,[Na]=4.5M, T=25•C and g/L=0.2

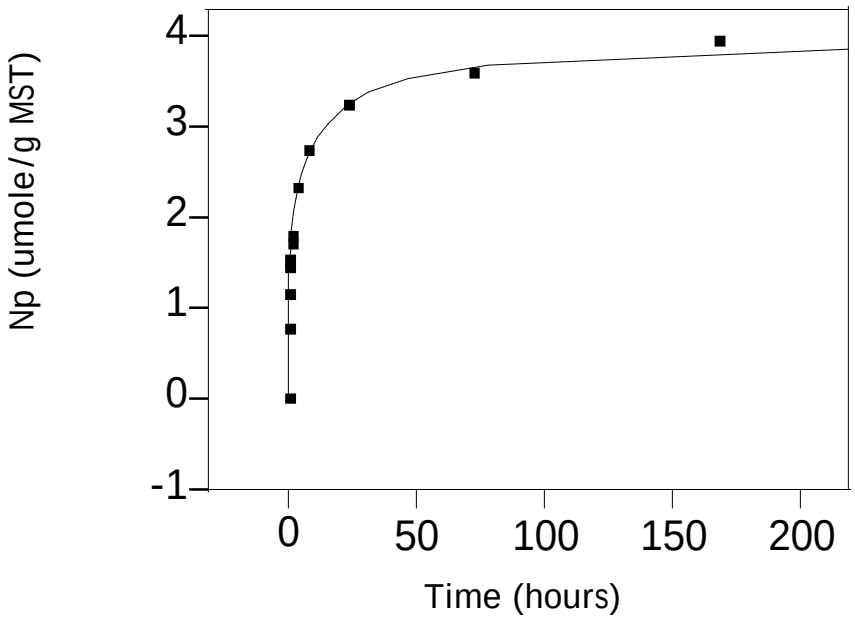

Figure E4. Np loading on MST at [OH]=1M,[Na]=4.5M, T=25•C and g/L=1.1

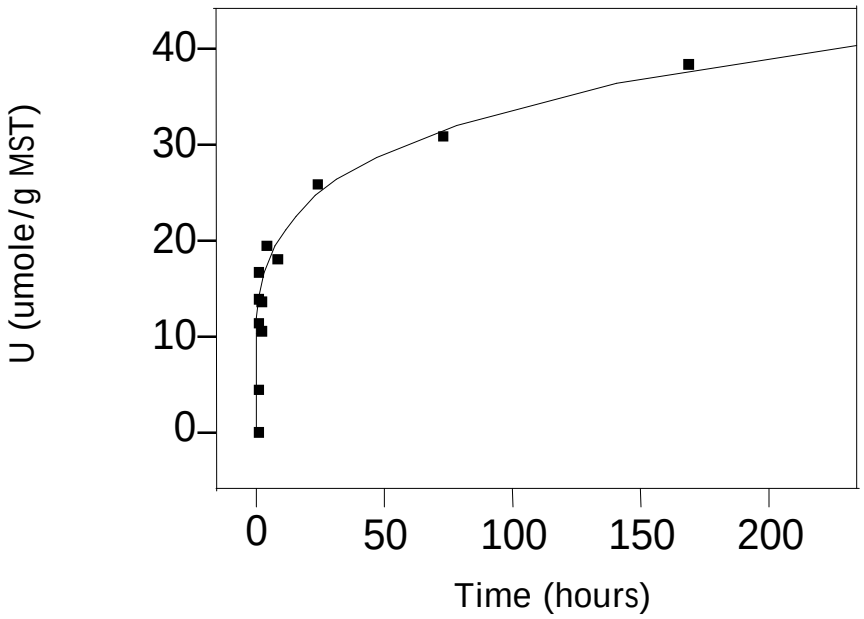

Figure E5. U loading on MST at [OH]=1.4M,[Na]=6M, T=25•C and g/L=0.2

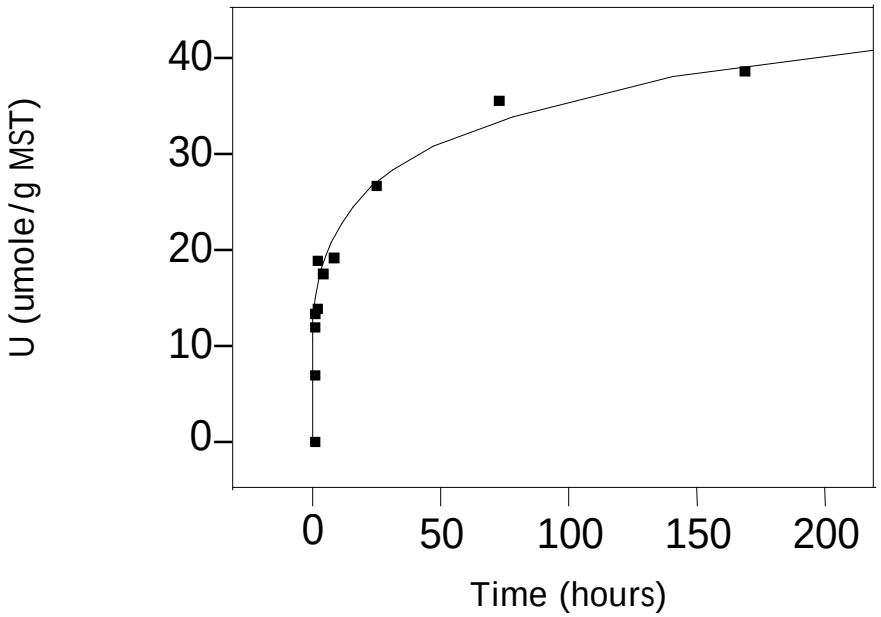

Figure E6. U loading on MST at [OH]=1.4M,[Na]=6M, T=25•C and g/L=1.1

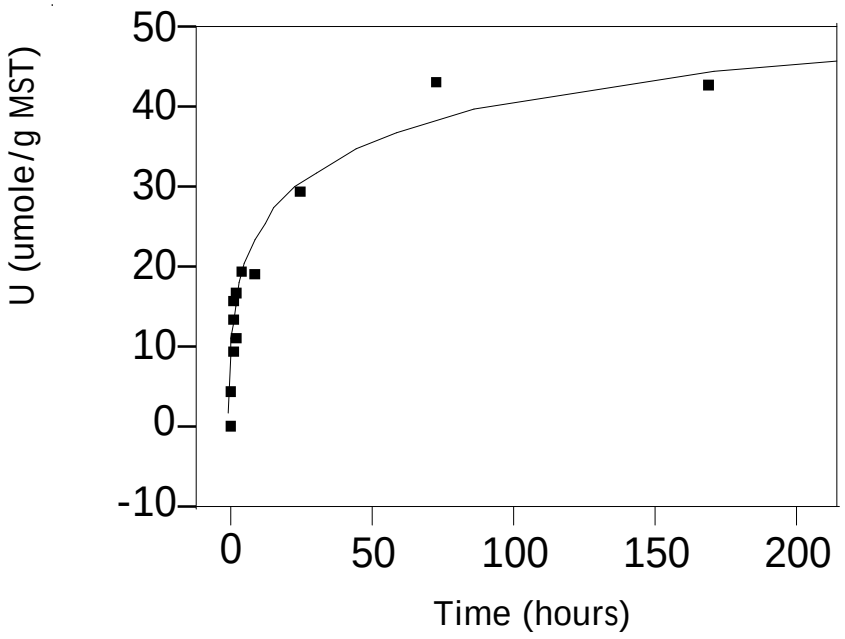

Figure E7. U loading on MST at [OH]=1M,[Na]=4.5M, T=25•C and g/L=0.2

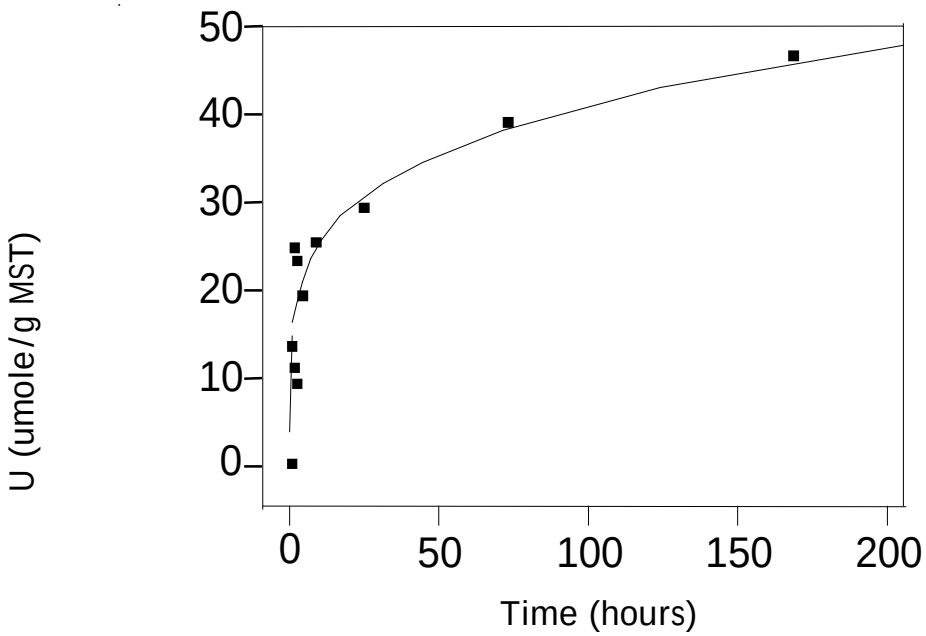

Figure E8. U loading on MST at [OH]=1M,[Na]=4.5M, T=25•C and g/L=1.1

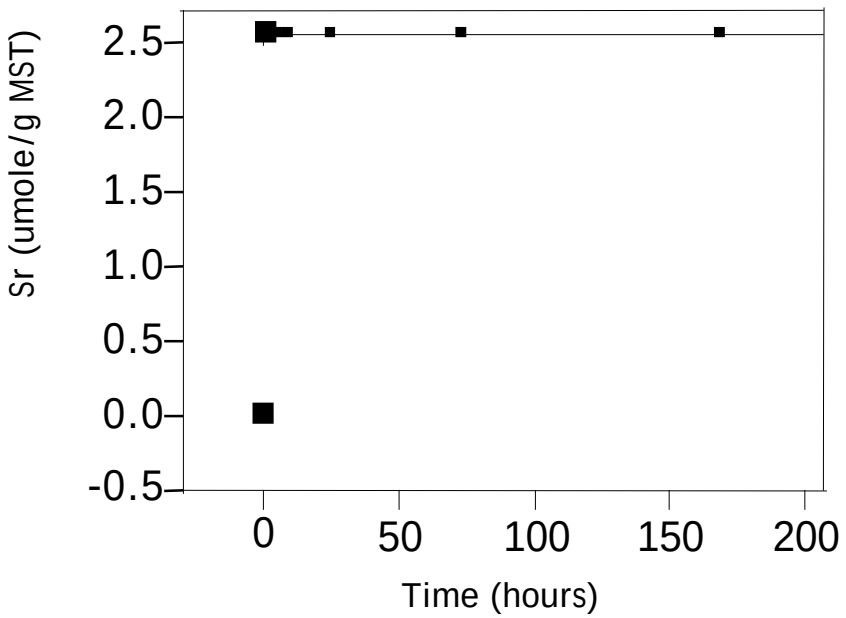

Figure E9. Sr loading on MST at [OH]=1.4M,[Na]=6M, T=25•C and g/L=0.2

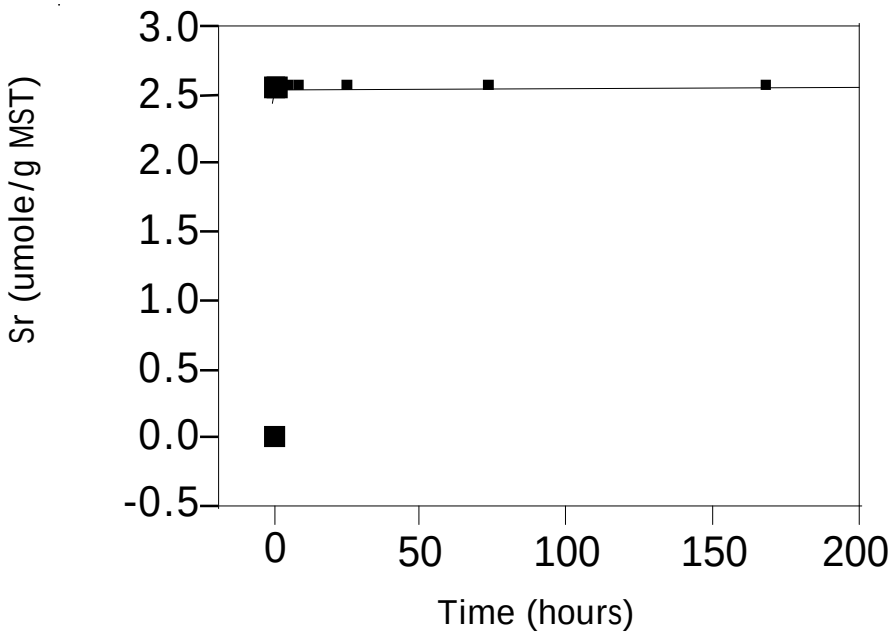

Figure E10. Sr loading on MST at [OH]=1.4M,[Na]=6M, T=25•C and g/L=1.1

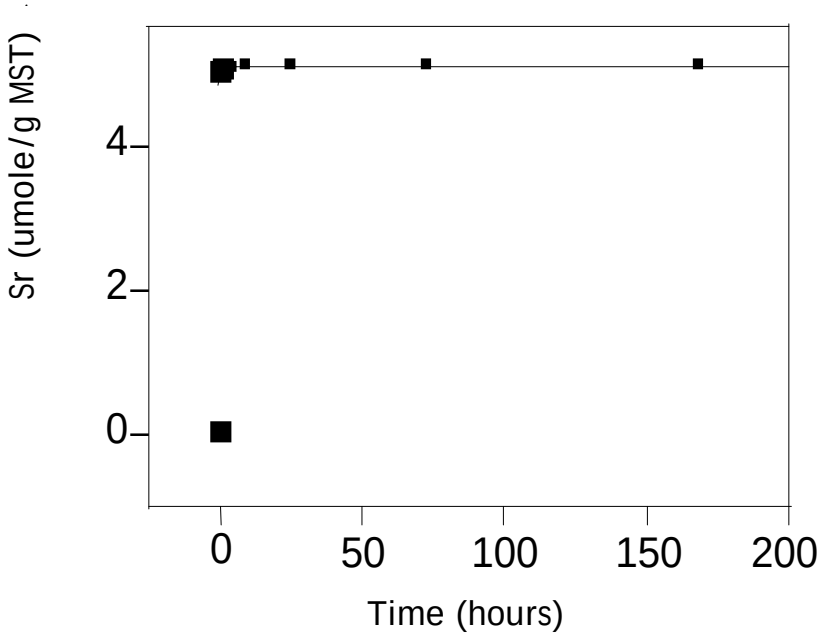

Figure E11. Sr loading on MST at [OH]=1M,[Na]=4.5M, T=25•C and g/L=0.2

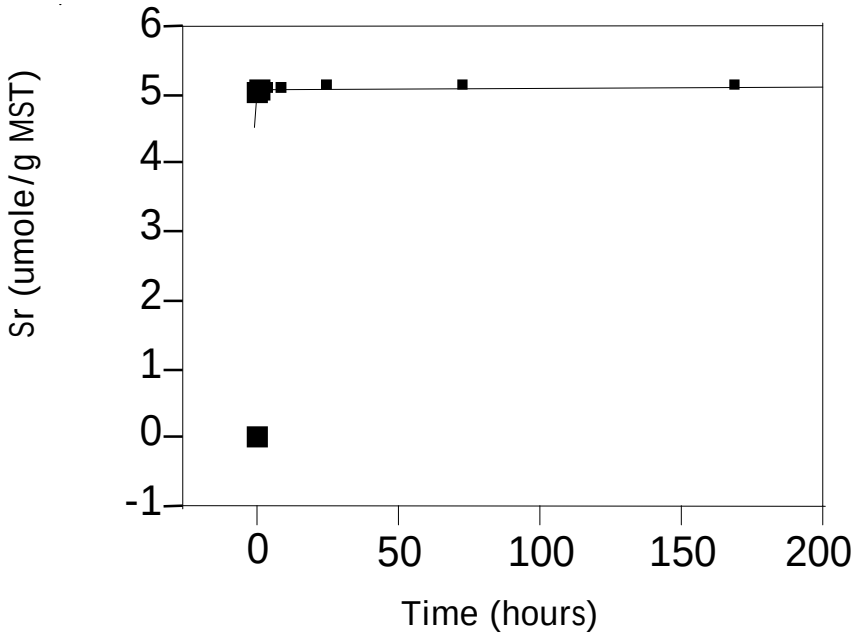

Figure E12. Sr loading on MST at [OH]=1M,[Na]=4.5M, T=25•C and g/L=1.1

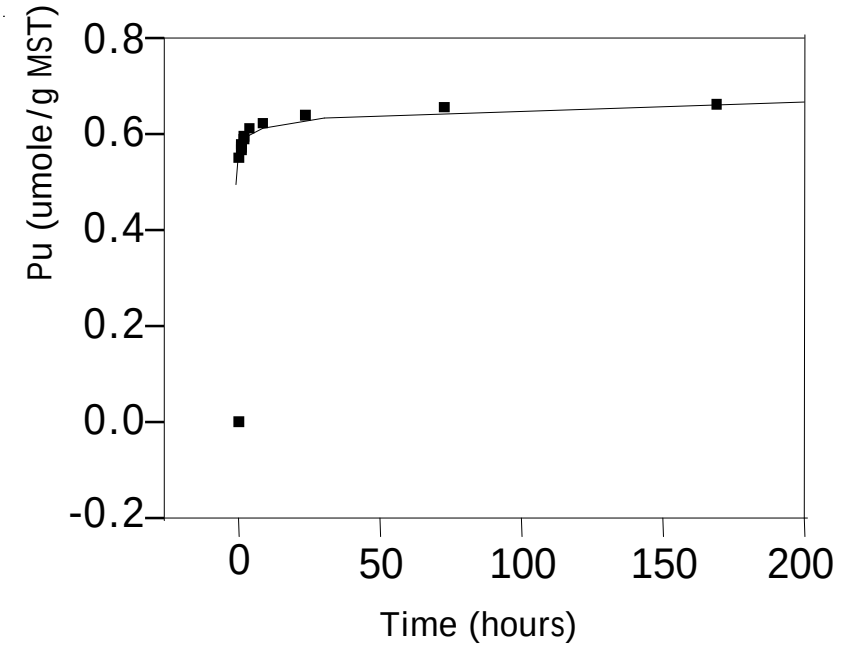

Figure E13. Pu loading on MST at [OH]=1.4M,[Na]=6M, T=25•C and g/L=0.2

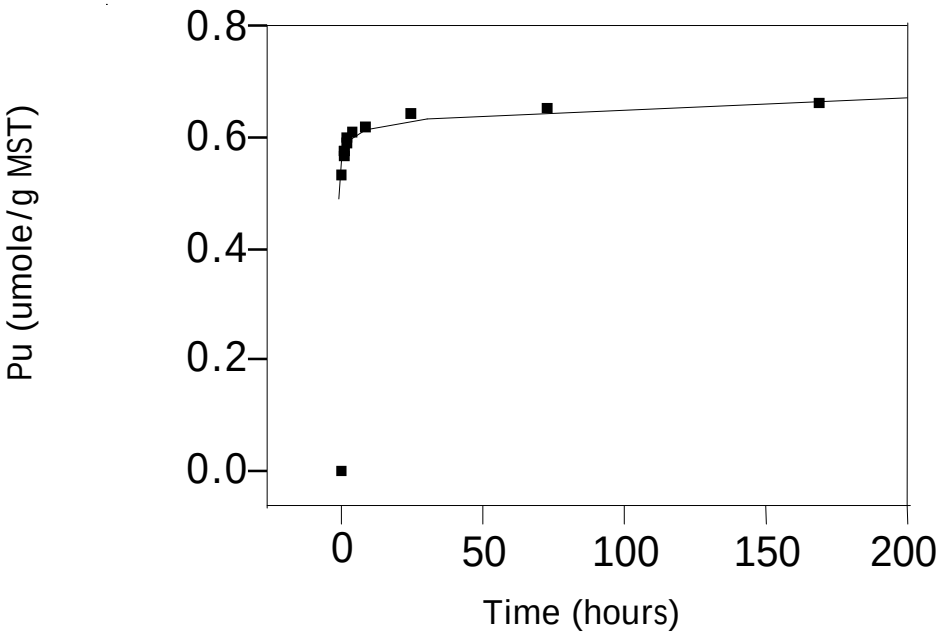

Figure E14. Pu loading on MST at [OH]=1.4M,[Na]=6M, T=25•C and g/L=1.1

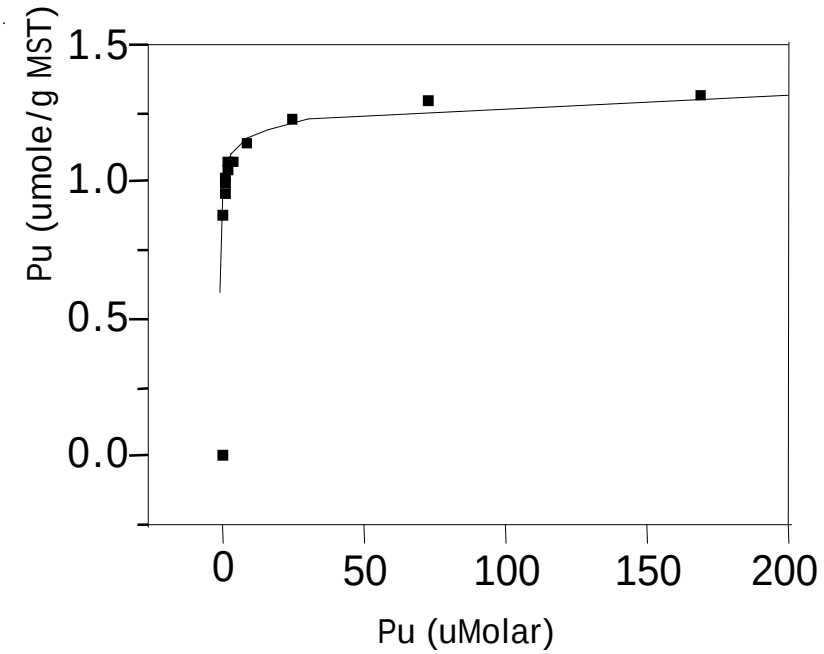

Figure E15. Pu loading on MST at [OH]=1M,[Na]=4.5M, T=25•C and g/L=0.2

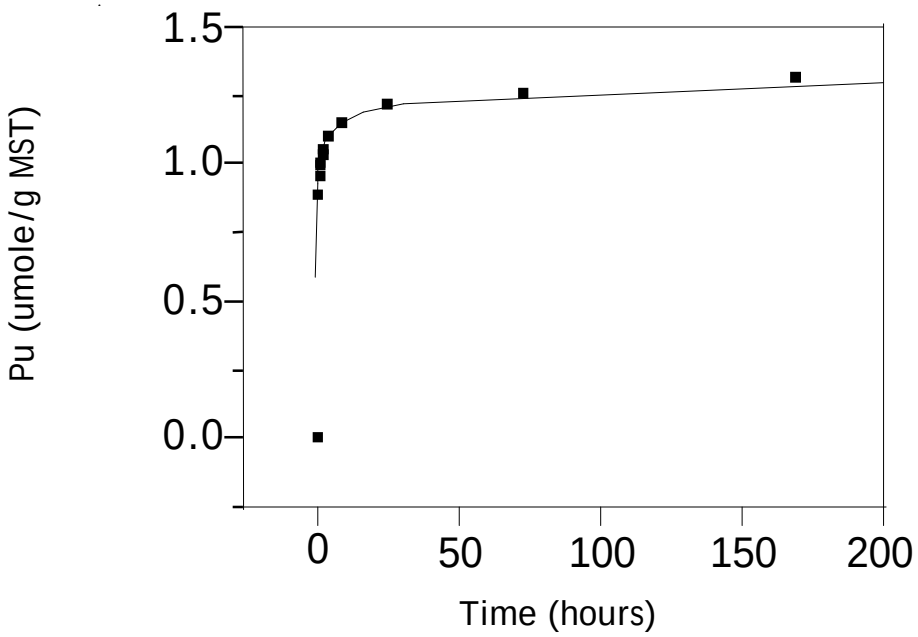

Figure E16. Pu loading on MST at [OH]=1M,[Na]=4.5M, T=25•C and g/L=1.1

Appendix F: Rahn Function Sensitivity Plots for Pu sorption on MST.

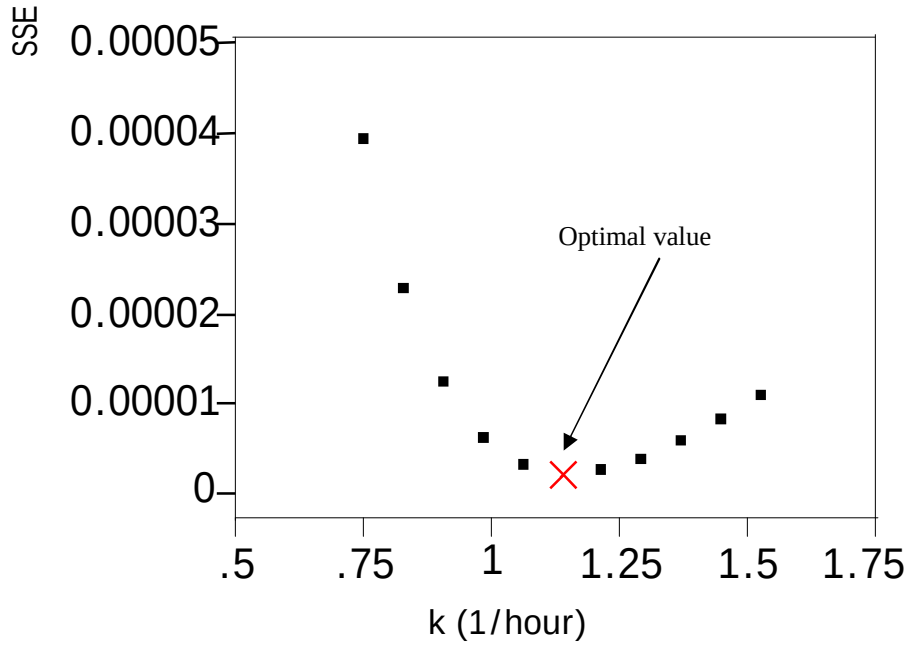

Figure F1. The sensitivity plot of the rate constant from Rahn's function

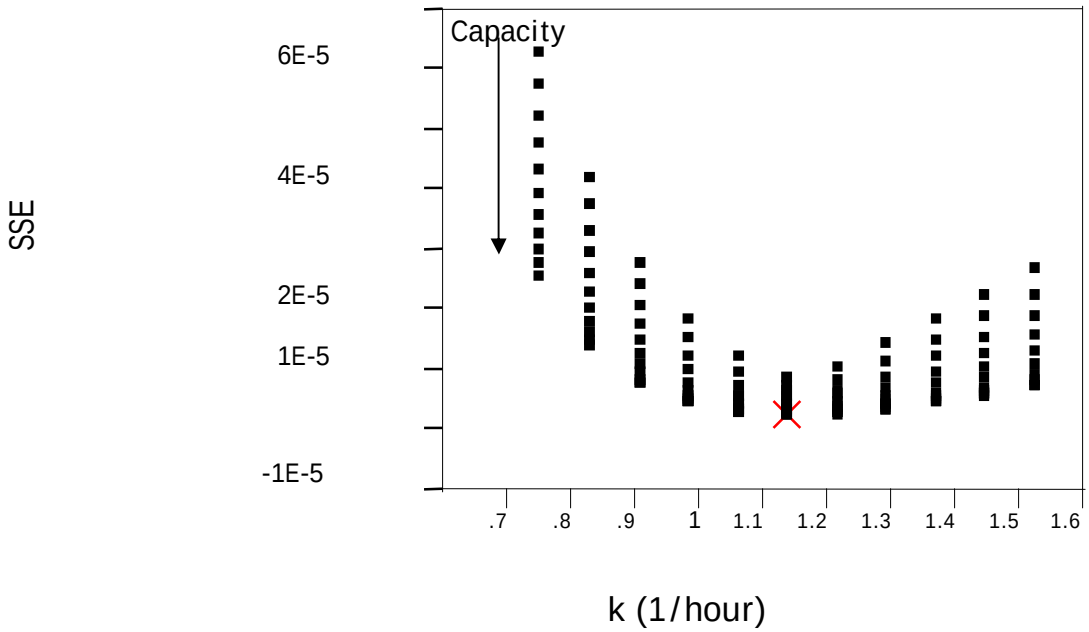

Figure F2. The sensitivity plot of the rate constant from Rahn's function at different MST capacities for Pu.

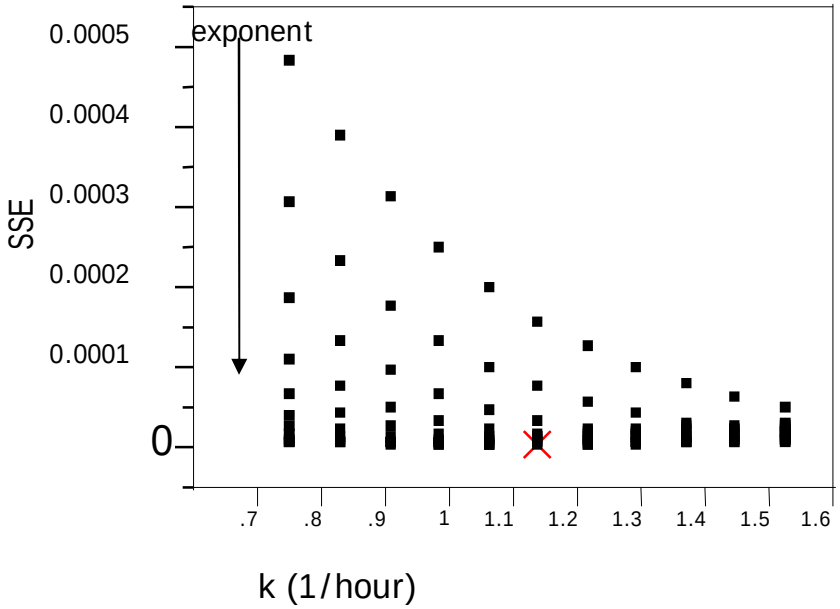

Figure F3. The sensitivity plot of the rate constant from Rahn's function at different exponent values.

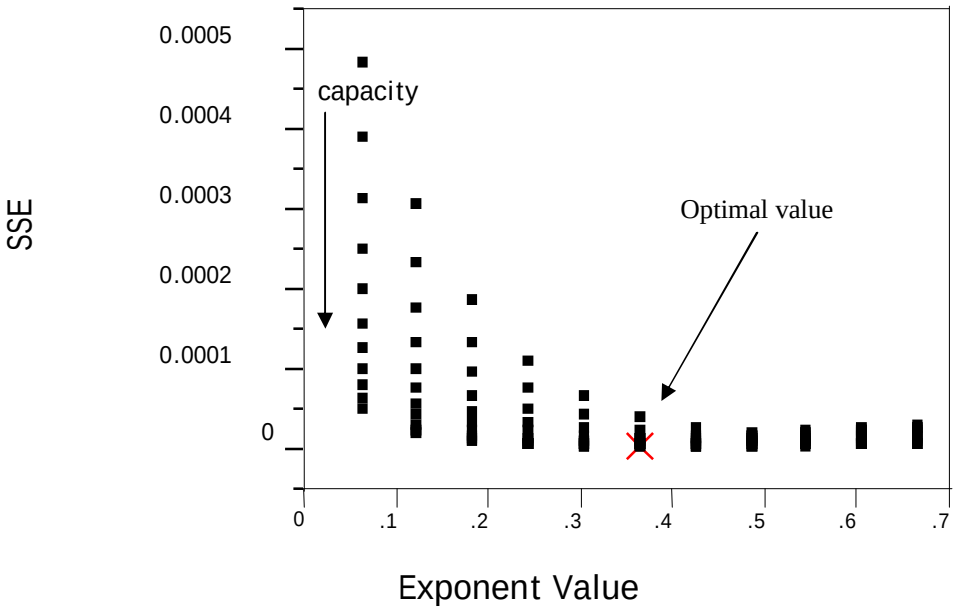

Figure F4. The sensitivity plot of the exponent constant from Rahn's function at different MST capacities for Pu.

Appendix G: Hyperbolic relationship between the rate constant and radionuclide capacity.

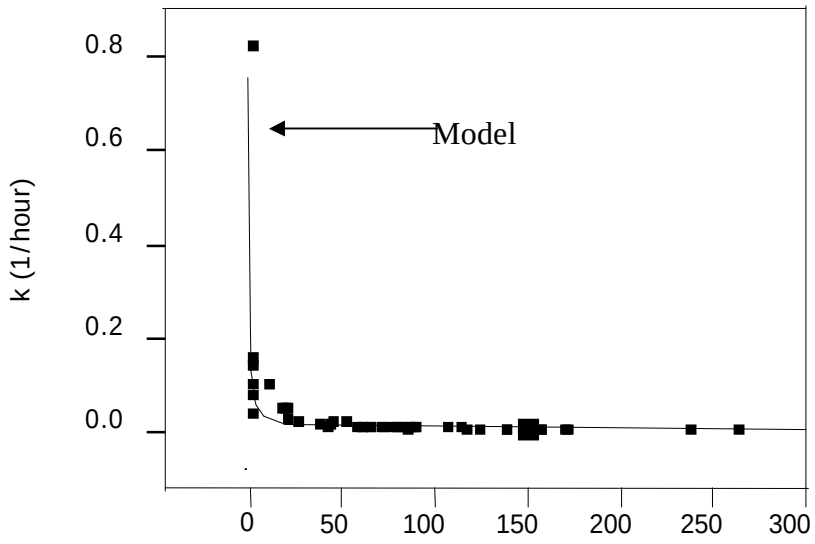

Figure G1. The rate constant from Rahn's function of MST capacities for Pu.

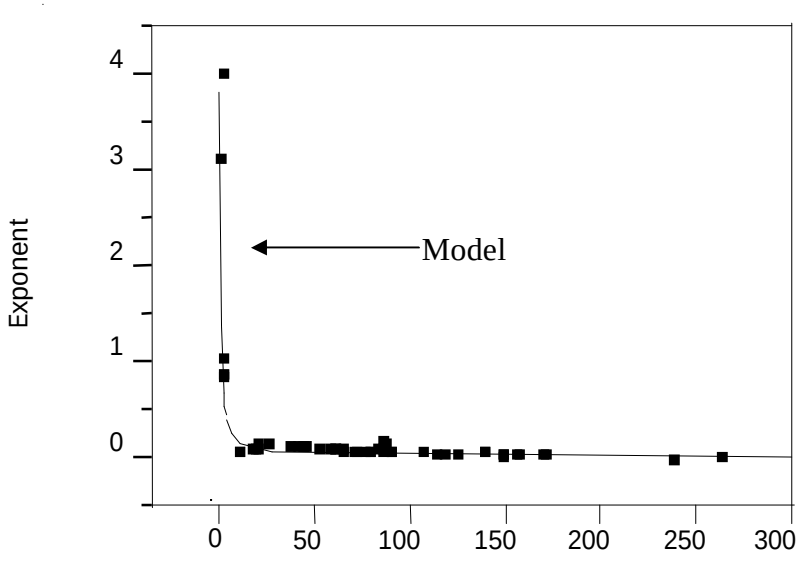

Figure G2. The exponent constant from Rahn's function at different MST capacities for Pu.

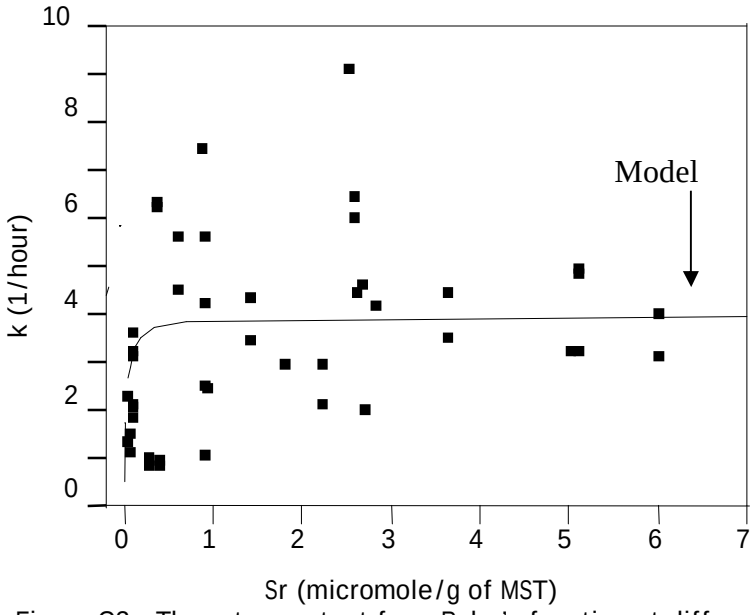

Figure G3. The rate constant from Rahn's function at different MST capacities for Sr.

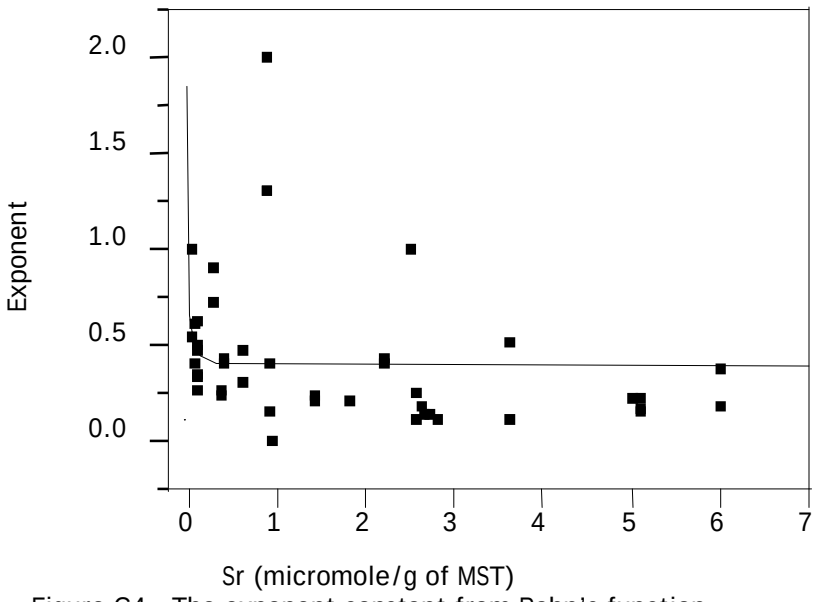

Figure G4. The exponent constant from Rahn's function at different MST capacities for Sr.

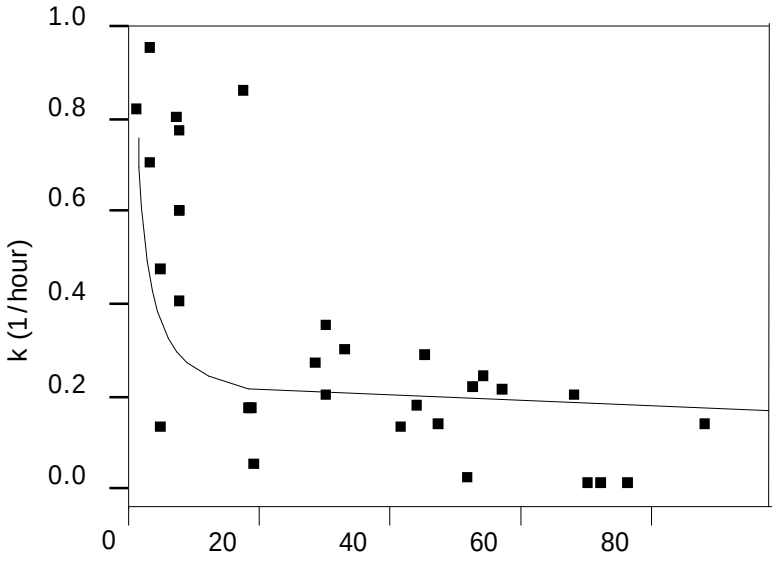

Figure G5. The rate constant from Rahn's function at different MST capacities for U.

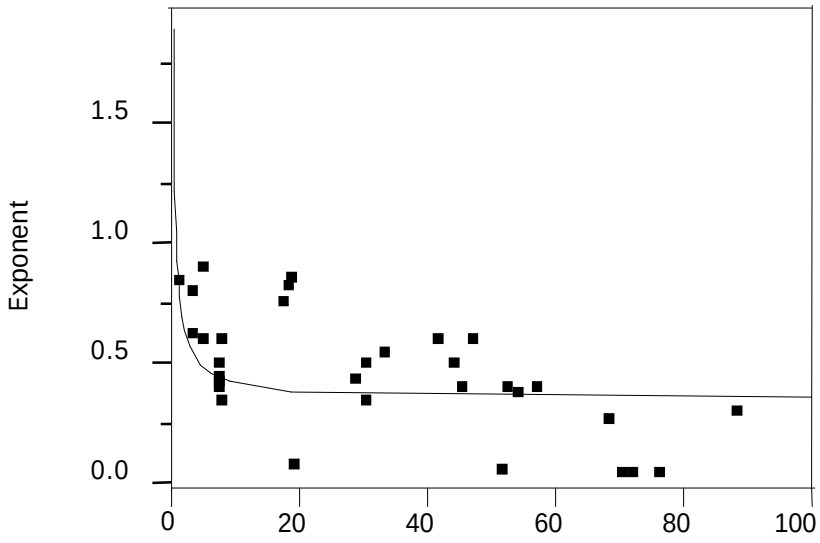

Figure G6. The exponent constant from Rahn's function at different MST capacities for U.

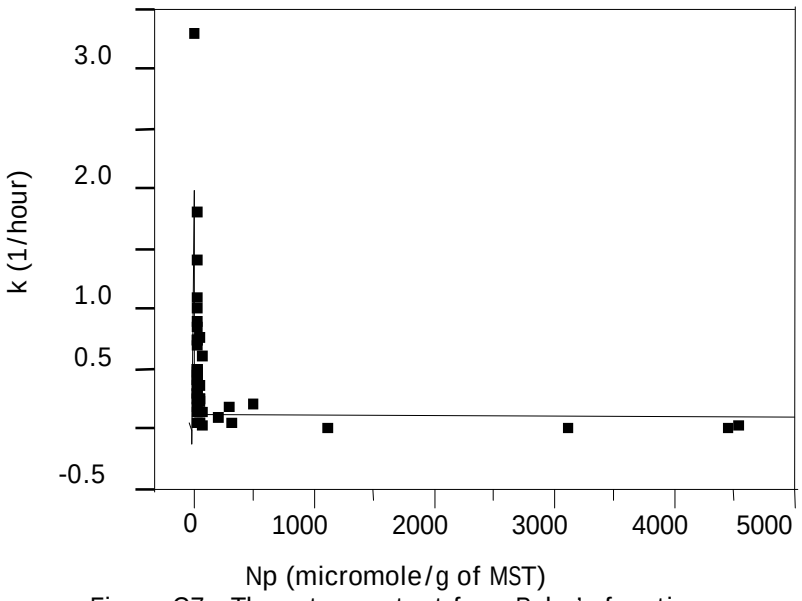

Figure G7. The rate constant from Rahn's function at different MST capacities for Np.

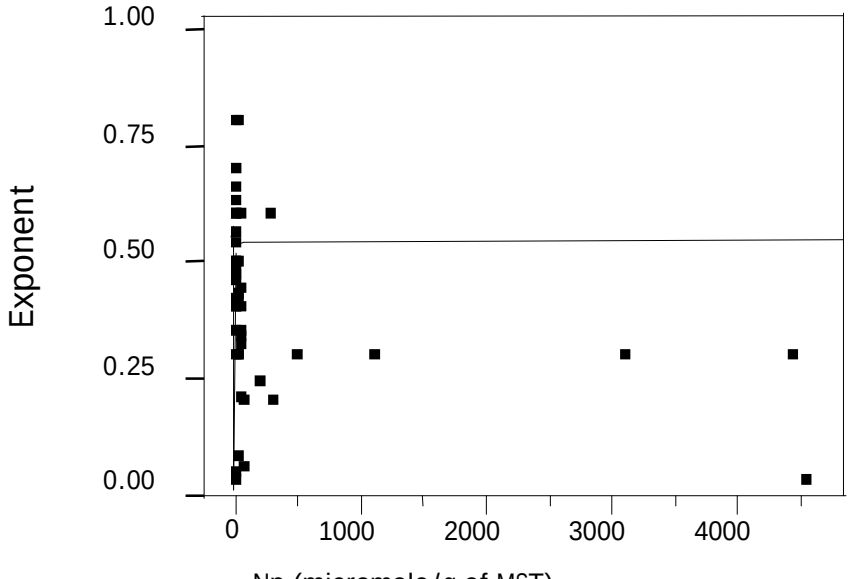

Figure G8. The exponent constant from Rahn's function at different MST capacities for Np.

Appendix H. The Rahn function parameters for the radionuclide sorption on MST.

Table H1. The Rahn function parameters for Pu loading data. Also shown is the hyperbolic relationship between the rate constant, exponent and capacity.

Index	Capacity (micromole/g MST)	Rate Constant (1/hour)	Exponent	Rate = a/capacity + b	Exponent= a/capacity + b
1	149	0.0066	0.008	0.013	0.024
2	238	0.005	-0.03	0.013	0.020
3	1	0.04	4	0.230	1.816
4	60	0.01	0.08	0.015	0.041
5	1	0.1	0.81	0.219	1.726
6	1	0.16	0.84	0.219	1.726
7	17	0.05	0.08	0.024	0.113
8	20	0.05	0.08	0.022	0.100
9	45	0.02	0.11	0.016	0.051
10	87	0.01	0.13	0.014	0.032
11	10	0.1	0.04	0.033	0.184
12	10	0.1	0.05	0.033	0.184
13	19	0.05	0.08	0.023	0.103
14	52	0.02	0.06	0.016	0.046
15	82	0.01	0.06	0.014	0.034
16	1	0.14	3.1	0.250	1.982
17	26	0.02	0.13	0.020	0.080
18	76	0.01	0.05	0.015	0.035
19	1	0.82	0.84	0.232	1.835
20	20	0.026	0.13	0.022	0.098
21	85	0.005	0.15	0.014	0.033
22	60	0.01	0.08	0.015	0.041
23	41	0.01	0.11	0.017	0.054
24	156	0.006	0.02	0.013	0.024
25	86	0.009	0.04	0.014	0.033
26	138	0.006	0.03	0.013	0.025
27	58	0.01	0.075	0.015	0.042
28	37	0.017	0.1	0.017	0.059
29	138	0.006	0.03	0.013	0.025
30	85	0.009	0.06	0.014	0.033

31	43	0.015	0.09	0.017	0.052
32	70	0.01	0.05	0.015	0.037
33	72	0.01	0.05	0.015	0.036
34	124	0.007	0.02	0.013	0.026
35	114	0.008	0.02	0.014	0.028
36	79	0.01	0.04	0.014	0.034
37	65	0.01	0.03	0.015	0.039
38	106	0.008	0.03	0.014	0.029
39	89	0.009	0.042	0.014	0.032
40	117	0.007	0.02	0.014	0.027
41	149	0.006	0.007	0.013	0.024
42	157	0.006	0.008	0.013	0.024
43	148	0.006	-0.005	0.013	0.024
44	263	0.004	-0.022	0.013	0.019
45	169	0.006	0.007	0.013	0.023
46	171	0.006	0.007	0.013	0.023
47	65	0.011	0.07	0.015	0.039
48	1	0.08	1.02	0.219	1.726
49	89	0.009	0.04	0.014	0.032
50	79	0.01	0.04	0.014	0.034

Table H2. The Rahn function parameters for Sr loading data. Also shown is the hyperbolic relationship between the rate constant, exponent and capacity.

Index	Capacity (micromole/g MST)	Rate Constant (1/hour)	Exponent	Rate = a/capacity + b	Exponent= a/capacity + b
1	0.860	7.4	1.3	3.867	1.146
2	0.880	1.04	2	3.869	1.128
3	0.880	2.5	1.3	3.869	1.128
4	0.930	2.4	-0.004	3.874	1.086
5	0.900	5.6	0.152	3.871	1.111
6	0.900	4.2	0.4	3.871	1.111
7	0.070	2.03	0.5	2.739	10.036
8	0.070	3.6	0.34	2.739	10.036
9	0.070	1.8	0.62	2.739	10.036
10	0.070	2.1	0.46	2.739	10.036
11	0.070	3.2	0.26	2.739	10.036
12	0.070	3.1	0.32	2.739	10.036
13	0.270	1	0.72	3.648	2.867
14	0.270	0.8	0.9	3.648	2.867
15	3.620	4.4	0.11	3.943	0.545
16	3.610	3.5	0.51	3.943	0.546
17	0.028	2.24	0.54	0.898	24.553
18	0.028	1.29	1	0.898	24.553
19	0.360	6.3	0.23	3.728	2.240
20	0.360	6.2	0.26	3.728	2.240
21	0.390	0.9	0.4	3.746	2.095
22	0.390	0.83	0.42	3.746	2.095
23	6.000	3.1	0.37	3.952	0.471
24	6.000	4	0.18	3.952	0.471
25	0.050	1.1	0.6	2.248	13.907
26	0.050	1.5	0.4	2.248	13.907
27	0.600	4.5	0.47	3.823	1.487
28	0.600	5.6	0.3	3.823	1.487
29	2.560	6	0.1	3.933	0.623
30	2.560	6.4	0.24	3.933	0.623
31	5.100	4.8	0.15	3.867	1.146

32	5.100	4.9	0.16	3.869	1.128
33	2.200	2.9	0.43	3.869	1.128
34	2.200	2.1	0.4	3.874	1.086
35	1.400	3.4	0.2	3.871	1.111
36	1.400	4.3	0.23	3.871	1.111
37	5.100	3.2	0.22	2.739	10.036
38	5.000	3.2	0.22	2.739	10.036
39	2.600	4.5	0.15	2.739	10.036
40	2.600	4.4	0.17	2.739	10.036
41	2.650	4.6	0.13	2.739	10.036
42	2.500	9.1	1	2.739	10.036
43	1.800	2.9	0.2	3.648	2.867
44	2.700	2	0.13	3.648	2.867
45	2.800	4.12	0.11	3.943	0.545

Table H3. The Rahn function parameters for U loading data. Also shown is the hyperbolic relationship between the rate constant, exponent and capacity.

Index	Capacity (micromole/g MST)	Rate Constant (1/hour)	Exponent	Rate = a/capacity + b	Exponent= a/capacity + b
1	88.00	0.14	0.30	0.17	0.37
2	47.00	0.14	0.60	0.18	0.37
3	52.00	0.22	0.40	0.18	0.37
4	45.00	0.29	0.40	0.18	0.37
5	57.00	0.21	0.40	0.18	0.37
6	44.00	0.18	0.50	0.19	0.37
7	7.00	0.60	0.40	0.30	0.45
8	7.00	0.80	0.45	0.30	0.45
9	7.00	0.60	0.42	0.30	0.45
10	8.00	0.40	0.60	0.30	0.45
11	8.00	0.77	0.35	0.30	0.45
12	7.00	0.60	0.50	0.30	0.45
13	18.00	0.17	0.86	0.22	0.39
14	18.00	0.17	0.82	0.22	0.40
15	19.00	0.05	0.08	0.22	0.39
16	52.00	0.02	0.06	0.18	0.37
17	3.00	0.95	0.62	0.48	0.57
18	3.00	0.70	0.80	0.49	0.57
19	30.00	0.35	0.35	0.20	0.38
20	28.00	0.27	0.43	0.20	0.38
21	76.00	0.01	0.05	0.18	0.37
22	1.00	0.82	0.84	1.25	1.08
23	195.00	0.01	1.30	0.17	0.36
24	233.00	0.10	0.60	0.17	0.36
25	5.00	0.47	0.60	0.39	0.51
26	5.00	0.13	0.90	0.39	0.51
27	42.00	0.13	0.60	0.19	0.37
28	441.00	0.02	0.30	0.16	0.36
29	158.00	0.08	0.24	0.17	0.36
30	68.00	0.20	0.27	0.18	0.37
31	54.00	0.24	0.38	0.18	0.37

32	2.6E+04	0.00	0.21	0.16	0.36
33	5.8E+03	0.01	0.06	0.16	0.36
34	4.5E+03	0.01	0.03	0.16	0.36
35	70.00	0.01	0.05	0.18	0.37
36	72.00	0.01	0.05	0.18	0.37
37	124.00	0.01	0.02	0.17	0.36
38	114.00	0.01	0.02	0.17	0.36
39	26.00	0.70	1.17	0.20	0.38
40	33.00	0.30	0.55	0.19	0.38
41	4.1E+04	0.00	0.36	0.16	0.36
42	1.3E+04	0.00	0.32	0.16	0.36
43	9.5E+09	0.00	0.40	0.16	0.36
44	4.5E+07	0.00	0.20	0.16	0.36
45	17.00	0.86	0.76	0.22	0.40
46	1.4E+04	0.00	0.14	0.16	0.36
47	4.0E+05	0.00	0.14	0.16	0.36
48	30.00	0.20	0.50	0.20	0.38
49	31.00	0.01	1.40	0.20	0.38
50	35.00	0.01	1.65	0.19	0.38
51	39.00	0.02	1.20	0.19	0.38
52	27.00	0.01	1.40	0.20	0.38
53	88.00	0.14	0.30	0.17	0.37

Table H4. The Rahn function parameters for Np loading data. Also shown is the hyperbolic relationship between the rate constant, exponent and capacity.

Index	Capacity (micromole/g MST)	Rate Constant (1/hour)	Exponent	Rate = a/capacity + b	Exponent= a/capacity + b
1	37	0.05	4	0.170	0.543
2	47	0.14	0.6	0.158	0.545
3	38	0.75	0.34	0.168	0.543
4	35	0.04	0.4	0.173	0.543
5	50	0.6	0.2	0.155	0.545
6	194	0.09	0.24	0.124	0.549
7	4	1.1	0.4	0.640	0.484
8	4	1.8	0.3	0.640	0.484
9	4	1	0.6	0.627	0.485
10	4	0.7	0.7	0.627	0.485
11	4	1.4	0.6	0.640	0.484
12	4	0.85	0.8	0.640	0.484
13	7	0.24	1.6	0.428	0.511
14	7	0.9	0.5	0.423	0.511
15	19	0.05	0.08	0.224	0.536
16	52	0.02	0.06	0.154	0.545
17	1	3.3	0.05	3.126	0.171
18	3	0.3	0.03	0.866	0.455
19	30	0.35	0.35	0.183	0.541
20	33	0.23	0.32	0.176	0.542
21	45	0.24	0.21	0.160	0.544
22	27	0.14	0.8	0.191	0.540
23	279	0.17	0.6	0.120	0.549
24	487	0.19	0.3	0.117	0.550
25	3	0.74	0.5	0.752	0.470
26	3	0.45	0.7	0.752	0.470
27	36	0.25	0.44	0.171	0.543
28	298	0.04	0.2	0.120	0.549
29	4	0.5	0.4	0.640	0.484
30	4	0.5	0.5	0.640	0.484
31	7	0.35	0.43	0.402	0.514

32	7	0.4	0.42	0.432	0.510
33	4	0.46	0.46	0.592	0.490
34	4530	0.014	0.03	0.113	0.550
35	3	0.4	0.47	0.894	0.452
36	3	0.74	0.35	0.924	0.448
37	6	0.3	0.63	0.464	0.506
38	6	0.3	0.66	0.464	0.506
39	4	0.4	0.4	0.640	0.484
40	4	0.4	0.56	0.683	0.478
41	4	0.35	0.48	0.603	0.488
42	6	0.5	0.42	0.448	0.508
43	3	0.25	0.54	0.752	0.470
44	1090	0.0006	0.3	0.115	0.550
45	8	0.18	0.3	0.390	0.515
46	7	0.14	0.3	0.406	0.513
47	3100	0.0003	0.3	0.114	0.550
48	4430	0.0002	0.3	0.113	0.550

5.0 **References**

[1] Peters, T. B., Fink, S. D., Hobbs, D. T., Norato, M. A., and Walker, D. D., "Demonstration of MST and Permanganate Efficiency on Removal of Actinides and Strontium from Savannah River Site High Level Waste," WSRC-TR-2002-00255, March 11, 2003.

[2] F. F. Fondeur, D. T. Hobbs, M. J. Barnes and S. D. Fink, " Sorption Modeling of Sr, Pu, U and Np adsorption on Monosodium Titanate," WSRC-TR-2003-00180, May 2003.

[3] Poirier, M. R., Herman, D. T., Burkett, P. R., Peters, T. B., Serkiz, S. M., and Fink, S. D., "Testing of the Insitu Mixed-Iron Oxide (ISMIO) Alpha Removal Process," WSRC-TR-2004-00283, June 29, 2004.

[4] Barnes, M. J., F. F. Fondeur, D. T. Hobbs, and S. D. Fink, "Monosodium Titanate Multi-Strike Testing," WSRC-TR-2004-00145, April 29, 2004.

[5] M. M. Dubinin and L. V. Radushkevich, "Equation of the Characteristic Curve of Activated Charcoal," Chem. Zentr Vol. 1(1947), p. 875.

[6] G.F. Forment and K. B. Bischoff, "Chemical Reactor Analysis and Design," John wiley & Sons, Inc. 1990.

[7] Rudzinski, W. and Panczyk, T, "Kinetics of Isothermal Adsorption on Energetically Heterogeneous Solid Surfaces: A New Theoretical Description Based on the Statistical Rate Theory of Interfacial Transport," J. Phys. Chem. B, 2000, 104, PP 9149-9162.

[8] Azizian, S., "Kinetics Models of Sorption: a Theoretical Analysis," J. Coll. and Int. Sc., 2004, 276, PP 47-52.

[9] Cheung, C. W., Porter, J. F., and McKay, G., "Sorption Kinetic Analysis for the Removal of Cadmium Ions from Effluents Using Bone Char," Wat. Res., 2001, 35, PP 605-612.

[10] Georgiadis, R., Peterlinz, K. P., and Peterson, A. W., " Quantitative Measurements and Modeling of Kinetics in Nucleic Acid Monolayer Films Using SPR Spectroscopy," J. Am. Chem. Soc., 2000, 122, PP. 3166-3173.

[11] Sag, Y. and Aktay, Y, "Kinetic Studies on Sorption of Cr(VI) and Cu(II) ions by Chitin, Chitosan, and Rhizopus arrhizus," Biochemical Eng. J.,2002, 12, PP. 143-153.

[12] Lazaridis, N. K., and Asouhidou, D. D., "Kinetics of Sorptive Removal of Chromium(VI) from Aqueous Solution by Clacined Mg-Al-CO3 hydrotalcite," Water Research, 2003, 37, PP. 2875-2882.

[13] Hibbert, D. B., Gooding, J. J., and Erokhin, P., "Kinetics of Irreversible Adsorption with Diffusion: Application to Biomolecule Immobilization," Langmuir, 2002, 18, PP 1770-1776.

[14] Barlow, K, Nash, D., Grayson, R, "Investigating Phosphorus Interactions with Bed Sediments in a Fluvial Environment using a Recirculating Flume and Intact Soil Cores," Water Research, 2004, 38, PP. 3420-3430.

[15] "Demonstration of MST Efficacy on Removal of Actinides and Strontium in Bounding Alpha Waste," S. D. Fink, D. T. Hobbs and T. B. Peters, WSRC-TR-2002-00555, December 2002

[16] Perry, J. H., Perry, R. H., Chilton, C. H., Kirkpatrick, S. D., "Chemical Engineers' Handbook", Fourth Edition, McGraw-Hill, 1963.

[17] Nakashima, S., "Diffusivity of Ions in Pore Water as a Quantitative Basis for Rock Deformation Rate Estimates," Tectonophysics, 1995, vol. 245, PP. 185-203.

[18] Walker, D., D., "Viscosity Measurements on Clear Liquids," WSRC-RP-93-294, February 9, 1993.

[19] Peters, T. B., Fink, S. D., Hobbs, D. T., Norato, M. A., and Walker, D. D., "Demonstration of MST and Permanganate Efficiency on Removal of Actinides and Strontium from Savannah River Site High Level Waste," WSRC-TR-2002-00255, March 11, 2003.

R. A.	Adams	241-162H, Rm. 4	**(E)**
J. W.	Barber	704-2H, Rm. 197	**(E)**
J. L.	Barnes	704-S, Rm. 19	**(E)**
M. J.	Barnes	SRNL	**(E)**
W. M.	Barnes	704-56H, Rm. 164	**(E)**
S. M.	Blanco	766-H. Rm. 2434	**(E)**
L. R.	Bragg	766-H, Rm. 2434	**(E)**
T. E.	Britt	742-4G, Rm. 3	**(E)**
H. L.	Bui	742-4G, Rm. 3	**(E)**
S. G.	Campbell	703-H, Rm. 107	**(E)**
L.	Carey	766-H, Rm. 2005A	**(E)**
J. T.	Carter	703-H, Rm 122	**(E)**
W. D.	Clark	766-H, Rm. 2412	**(E)**
S. L.	Clifford	766-H, Rm. 2443	**(E)**
J. J.	Connelly	773-41A, Rm. 231	**(E)**
D. T.	Conrad	766-H, Rm. 2007	**(E)**
D. R.	Cox	730-2B, Rm. 118	**(E)**
A. D.	Cozzi	773-43A, Rm. 218	**(E)**
C. L.	Crawford	773-41A, Rm. 180	**(E)**
D. A.	Crowley	SRNL	**(E)**
N. R.	Davis	766-H, Rm. 1006	**(E)**
W. B.	Dean	766-H, Rm. 2243	**(E)**
V. G.	Dickert	703-H, Rm. 4	**(E)**
C. L.	Donahue	241-162H, Rm. 6	**(E)**
M. D.	Drumm	766-H, Rm. 2050	**(E)**
M. C.	Duff	773-43A, Rm. 217	**(E)**
J. L.	Dunning	766-H, Rm. 2020	**(E)**
C. R.	Dyer	766-H, Rm. 2426	**(E)**
R. E.	Eibling	999-W, Rm. 335	**(E)**
G. N.	Eide	241-121H, Rm. 6	**(E)**
H. H.	Elder	703-H, Rm. 95	**(E)**
S. D.	Fink	SRNL	**(E, P)**
F. F.	Fondeur	SRNL	**(E)**
R. C.	Fowler	703-H, Rm. 98	**(E)**
L. M.	Fox	703-H, Rm. 3	**(E)**
M.W.	Geeting	766-H, Rm. 2035	**(E)**
B. A.	Gifford	766-H, Rm. 1066D	**(E)**
A. P.	Giordano	703-H, Rm 79	**(E)**
J. C.	Griffin	SRNL	**(E)**
B. A.	Hamm	766-H, Rm. 2237	**(E)**
H. D.	Harmon	766-H, Rm. 2014	**(P)**
K. D.	Harp	755-H, Rm. 1066B	**(E)**
E. W.	Harrison	766-H, Rm. 2034	**(E)**
K. A.	Hauer	703-H, Rm. 11	**(E)**
D. T.	Herman	735-11A, Rm. 104	**(E)**
P. J.	Hill	766-H, Rm. 1066C	**(E)**
R. N.	Hinds	766-H, Rm. 2430	**(E)**
D. T.	Hobbs	SRNL	**(E)**
E. W.	Holtzscheiter	SRNL	**(E)**
C. M.	Jantzen	SRNL	**(E)**
R. T.	Jones	766-H, Rm. 2463	**(E)**
E. T.	Ketusky	703-H, Rm. 83	**(E)**
D. P.	Lambert	SRNL	**(E)**
C. A.	Lanigan	766-H, Rm. 2440B	**(E)**
C. A.	Langton	773-43A, Rm. 219	**(E)**
T. T.	Le	766-H, Rm. 2237	**(E)**
R. K.	Leugemors	766-H,	**(E)**
D. B.	Little	703-H, Rm. 3	**(E)**
S. R.	Loflin	773-41A, Rm. 223	**(E)**
N. P.	Malik	704-26F, Rm. 11	**(E)**
J. C.	Marra	773-42A, Rm. 173	**(E)**
D. J.	Martin	703-H, Rm. 84	**(E)**
K. B.	Martin	773-42A, Rm. 14	**(E)**
C. J.	Martino	735-11A, Rm. 121	**(E)**
G. J.	Matis	766-H, Rm. 1066F	**(E)**
D.	Maxwell	766-H, Rm. 2231	**(E)**
D. J.	McCabe	773-42A, Rm. 153	**(E)**
J. W.	McCullough	766-H, Rm. 2411	**(E)**
L. T.	McGuire	766-H, Rm. 2441	**(E)**
M. S.	Miller	772-7B, Rm. 6	**(E)**
C. A.	Nash	773-42A, Rm. 182	**(E)**
L. M.	Nelson	773-43A, Rm. 222	**(E)**
M. A.	Norato	704-27S, Rm. 6	**(E)**
M. R.	Norton	766-H, Rm. 2002	**(E)**
J. E.	Occhipinti	704-S, Rm. 18	**(E)**
L. D.	Olson	703-H, Rm. 5	**(E)**
L. M.	Papouchado	SRNL	**(P)**
T. B.	Peters	773-42A, Rm. 128	**(E)**
J. A.	Pike	703-H, Rm. 99	**(E)**
M. R.	Poirier	773-42A, Rm. 123	**(E)**
S. H.	Reboul	703-H, Rm. 84	**(E)**
T. R.	Reynolds	704-S, Rm. 65	**(E)**
M.A.	Rios-Armstrong	766-H, Rm 2054	**(E)**
S. J.	Robertson	766-H, Rm. 2500	**(P)**
B. C.	Rogers	766-H, Rm. 2008	**(E)**
R. A.	Runnels	766-H, Rm. 2011	**(E)**
P. J.	Ryan	704-61S, Rm. 6	**(E)**
E.	Saldivar	766-H, Rm. 2004	**(E)**
S. C.	Shah	766-H, Rm. 2037	**(E)**
D. C.	Sherburne	704-S, Rm. 18	**(E)**
T. J.	Spears	766-H, Rm. 2015	**(E)**
R. H.	Spires	766-H, Rm. 2003	**(E)**
M. E.	Stallings	SRNL	**(E)**
W. E.	Stevens	SRNL	**(E)**
S. J.	Strohmeier	766-H, Rm. 2022	**(E)**
S. G.	Subosits	766-H, Rm. 2052	**(E)**
P. C.	Suggs	766-H, Rm. 2436	**(E)**
G. A.	Taylor	703-H, Rm. 96	**(E)**
S. A.	Thomas	766-H, Rm. 2016	**(E)**
P. J.	Valenti	730-4B, Rm. 2062	**(E)**
W. B.	Van-Pelt	704-S, Rm. 16	**(E)**
D. D.	Walker	SRNL	**(E)**
A. O.	Waring	766-H, Rm. 2423	**(E)**
F. A.	Washburn	766-H, Rm. 2054	**(E)**
V. B.	Wheeler	766-H, Rm. 2438	**(E)**
G. G.	Wicks	SRNL	**(E)**
W. R.	Wilmarth	773-42A, Rm. 171	**(E)**
G. C.	Whinship	766-H, Rm. 2024	**(E)**
LWP File		773-42A	**(E, P)**
STI		703-43A **(E) (P 3 copies)**	

***Our standard distribution format is electronic unless otherwise requested**

(E) Electronic

(P) Paper Mail